Chair of Computational Modeling and Simulation
TUM School of Engineering and Design
Technical University of Munich

A Knowledge-Driven Approach in Fabrication Information Modeling

Scientific work to obtain the degree

Master of Science (M.Sc.)

at the TUM School of Engineering and Design
of the Technical University of Munich.

Supervised by Prof. Dr-Ing. André Borrmann
M.Sc Martin Slepicka
M.Sc Chao Li
Chair of Computational Modeling and Simulation

Submitted by Yuri Larissa [redacted]

Submitted on August 15, 2024

Acknowledgement

I would like to express my deepest gratitude to my advisor Martin Slepicka, whose constant guidance throughout this journey has been invaluable. His profound works and deep interest in Fabrication Information Modeling have inspired me and enhanced my understanding on the topic. I truly appreciate his patience and constructive feedback, which have helped me advance at every step of the process.

Furthermore, I am sincerely grateful for my advisor Chao Li, This thesis would not have been possible without his dedication and support for the AMC knowledge base in this work. I am thankful for being able to explore and gained many new insights from his field. His comprehensive understanding and explanation have supported me in shaping this work.

I would also like to thank Maximilian Hechtl for providing valuable insights into the study of concrete printing materials. His expertise was essential for implementing the experimental study on testing the printing material.

Additionally, I would not have been able achieve my goals and passion without the unwavering guidance from Max Lörtzing. His constant support and belief in my capabilities have been a driving force of in my development.

Finally, I am remarkably indebted to my family for their unconditional love and belief in me. Their constant support has been the greatest source of strength. To my friends, for their companionship through good and challenging times.

Abstract

The application of Additive Manufacturing in Construction (AMC) requires thorough iterative planning to ensure the manufacturability and quality of the printed outputs. Often in the early design stages, designers encounter incomplete data or knowledge gaps, presenting challenges in overcoming the complexity of AMC methods. The study proposed by (Li et al., 2022) introduces a Design Decision Support System (DDSS) integrated with Additive Manufacturing (AM) ontology, facilitating informed decision-making on AM methods.

This research thereby integrates the AMC knowledge base and the Fabrication Information Modelling (FIM) framework (Slepicka et al., 2021) to develop a knowledge-driven planning method. This approach aims to minimize fabrication trial and error, and refine the design methodologies. This specifically involves retrieving appropriate process parameters through considering rheological behaviors of 3D concrete printing (3DCP) materials and providing a systematic assessment of reachability of the robot printer to estimate appropriate design scale; thus support the design decision in the early phase.

Zusammenfassung

Das additiven Fertigungsverfahren im Bauwesen erfordert gründliche iterative Planung, um die Machbarkeit und Qualität der gedruckten Ergebnisse zu gewährleisten. Oft stoßen Planner in den frühen Planungsphasen auf unvollständige Daten oder Wissenslücken, was Herausforderungen aufgrund der Komplexität von AMC-Methoden darstellt. Ein Design Decision Support System (Design-Entscheidungsunterstützungssystem) (LI et al., 2022), welches mit der Ontologie der additiven Fertigung integriert ist, soll den Planern eine Wissensbasis zur Verfügung stellen, auf deren Grundlage sie geeignete Entscheidungen bei der Planung der additiven Fertigungsverfahren auswählen können.

Im Rahmen dieser Thesis soll eine wissensbasierte Planungsmethode entwickelt wreden, für deren Umsetzung die AMC-Wissensbasis sowie das Framework zur Fertigungsinformationsmodellierung FIM (SLEPICKA et al., 2021) integriert werden. Dieser Ansatz zielt darauf ab, Fehlversuche bei der Fertigung zu vermeiden und den Entwurfsprozess zu verbessern. Dies beinhaltet insbesondere die Ermittlung geeigneter Prozessparameter durch die Berücksichtigung des rheologischen Verhaltens von den 3D-Betondruckmaterialien und eine systematische Prüfung der Reichweite des gedruckten Roboters, um eine angemessene Designskalierung abzuschätzen und somit die Konstruktionsentscheidung in der frühen Phase zu unterstützen.

Contents

Abbreviations

3DCP	3D concrete printing
AEC	Architecture Engineering and Construction
AM	Additive Manufacturing
AMC	Additive Manufacturing in Construction
API	Application Programming Interface
BFO	Basic Formal Ontology
BIM	Building Information Modeling
CAD	Computer Aided Design
CAM	Computer Aided Manufacturing
CH	Calcium Hydroxide
CNC	Computer Numerical Control
CSH	Calcium Silicate Hydrate
DDSS	Design Decision Support System
DM	Digital Manufacturing
DOF	Degrees of Freedom
DOFs	Degrees of Freedoms
DUL	DOLCE+DnS Ultralite
FCM	Finite Cell Method
FIM	Fabrication Information Modelling
FP	Fast Penetration
IBS	Interlayer Bond Strength
IFC	Industry Foundation Class
IOF	Industrial Ontologies Foundry
KR	Knowledge Representation
OWL	Web Ontology Language
OWL2 DL	Web Ontology Language Description Logic
RDF	Resource Definition Framework

RPC Remote Procedure Calls

SP Slow Penetration

W3C World Wide Web Consortium

Chapter 1

Introduction

AMC has revolutionized the building industry by enabling the fabrication of complex geometries and automated construction through layer-by-layer material deposition based on 3D model data. Despite its potential and benefits, AMC requires thorough planning, involving detailed design iterations to ensure manufacturability and the quality of the printed products.

During the early design stages, uncertainties and incomplete information are common barriers that planners must overcome to face the complexity of detailed planning for AM methods. The DDSS introduced by Li et al. (2022) aims to support design decision process by providing a structured ontology consisting of heterogeneous domain knowledge related to AM. By integrating with Building Information Modeling (BIM), the DDSS provides geometry analysis, perform semantic retrieval and automatic inference, in which it incorporates semantic web technologies to create, update, and query formal knowledge. Thereby, the use of formalized knowledge provides early identification of suitable construction methods, ensuring the manufacturing capabilities.

Moreover, achieving a design-to-manufacturing process involves multiple work steps to acquire necessary data information for fabrication. It requires multiple conversions and data translations between designed model to AM tools which impose risk of data loss during conversion. FIM (Slepicka et al., 2022) addresses these challenges through implementing a continuous digital chain from design to production by automatically deriving manufacturing information from BIM data, effectively translating BIM models into print paths and machine control through the open exchange format Industry Foundation Class (IFC). Its information scope entails machine and process parameters, essential for executing AM processes.

Research Focus

Given the advantages of the AMC knowledge base and FIM, an opportunity arises for this research to explore the incorporation of both studies to develop a cohesive system that reduces trial and error, ensures compliance with design specifications. Thereby elevates the design process for AM methods in the early stages. This research seeks to explore how the AMC knowledge base can support the FIM framework by providing relevant data beneficial for fabrication.

In the early design phase for 3DCP, several considerations must be addressed to guarantee the viability of the construction. One key aspect is the selection of appropriate material compositions which entails properties that support extrudability, buildability, and

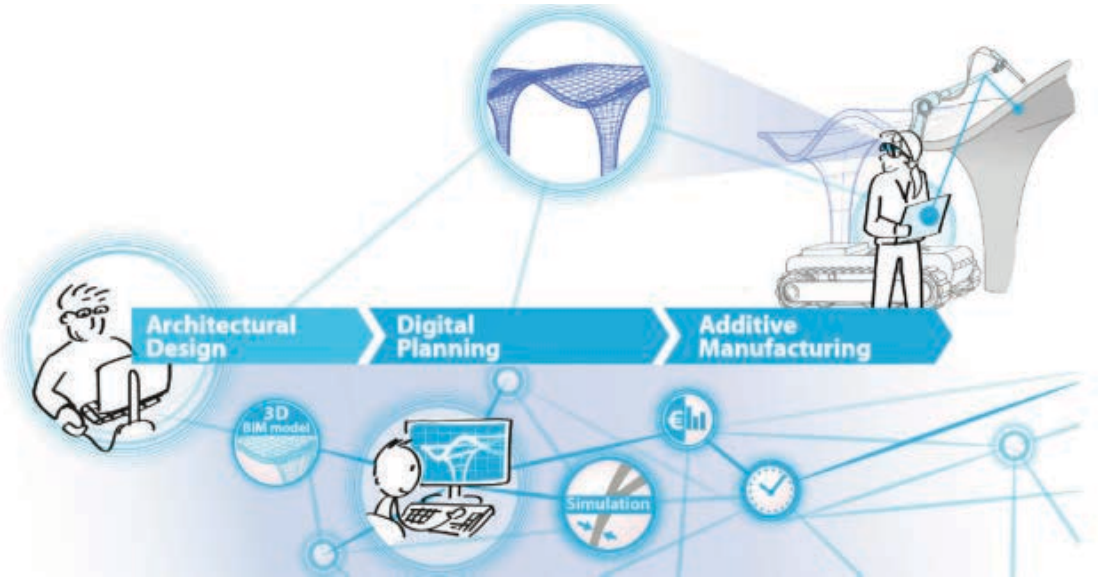

Figure 1.1: Digital process chain from planning to construction with AM technologies (KLOFT et al., 2021)

structural integrity during and after printing. Furthermore, the process parameters such as filament height, nozzle speed, and layer time significantly influences the quality of the printing outcome, in which the rheology properties of the material also play a role in the result. Nevertheless, addressing the potential limitation of design freedom related to scale is essential to predict the feasibility of intended design when choosing specific 3DCP methods.

With the aforementioned challenges, this provides the basis to define the scope for the master thesis. The study thereby focuses on retrieving appropriate process parameters through a knowledge driven approach specifically under consideration of the rheological behavior of 3DCP material. Ultimately, to identify feasibility in regards of the design scale, a manufacturability estimation is assessed to support the design in the early phase. To narrow down the focus area of the broad AMC technology, this research concentrates on the extrusion method using a stationary industrial robot (off-site printing), constructing planar vertical building elements.

Chapter 2

Theoretical Background

2.1 Additive Manufacturing in the Construction Industry

According to the international standard ISO/ASTM 52900 (2021), AM is defined as a process that involves printing materials layer-by-layer to produce components based on 3D model data. The first AM technology dates back to 1986 with Charles Hull's invention known as Stereolithigraphy. This paved the way for subsequent methods such as Powder Bed Fusion, Fused Deposition Modeling, Ink Jet Printing, and Contour Crafting. This innovation has been found across diverse industries including medical, transportation, and consumer products. Its integration within the construction sector however still remains in the early stages and under intensive research for its potential and challenges.

AM in construction has piqued interest in the Architecture Engineering and Construction (AEC) industry, representing a paradigm shift in construction methods. Its advantages include automated production process, enhanced design freedom, and reduced material consumption which traditional construction methods in comparison could not deliver. The automated process leads to reduction of construction time and labor costs, thereby enhancing the process efficiency (F. Bos et al., 2016).

2.1.1 Additive Construction Methods

The evolution of AM technology has introduced a myriad of possibilities for construction methods. Common strategies in the construction industry employ particle bed method and material extrusion, defined in the following:

Particle Bed Processes

Particle bed technologies entails a bed or chamber of dry material particles, typically aggregates in the construction sector. The process is followed by depositing liquid as binders into the chamber in horizontal layers, which then solidify to form the desired structure. After spraying, the final product becomes visible once the loose particles are removed. The solidified component is subsequently taken for sintering or heating to enhance its mechanical properties (Shakor et al., 2022).

Based on the material composition, this technology is distinguished into three techniques; (a) Selective Binder Activation: this method involves aggregates and binder (cement) within the bed. Solidification occurs as water is jetted onto the mixture, activating the

binder to construct the desired form. (b) Selective Paste Intrusion: paste comprising cement and water is sprayed into a bed of aggregates. (c) Binder Jetting: This technique is characterized by a bed that includes aggregates and a hardener, over which a liquid binder (resin) is sprayed (LOWKE et al., 2018).

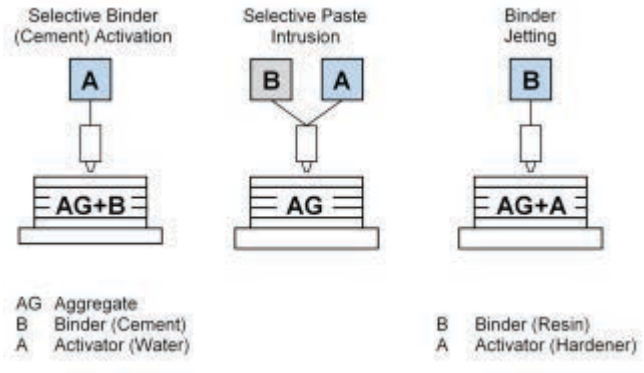

Figure 2.1: Particle Bed printing techniques (LOWKE et al., 2018)

This method offers the advantage to build complex geometries without supporting components, utilizing the support provided by the non-bonded particles. Overhangs are good example to be fabricated with particle bed technology without the necessity of additional framework. However, it is essential to consider the spatial requirements for construction space due to the required area for the particle bed.

Material Extrusion

Figure 2.2: Extrusion Method at Eindhoven University of Technology(PAOLINI et al., 2019)

In concrete extrusion, the process involves layerwise material deposition through a nozzle. This method heavily relies on material properties and printing parameters to ensure optimal quality of the end product. Key considerations for a successful material extrusion include

(1) ensuring the fluidity of the concrete to initiate flow, referred to as 'pumpability', (2) while also possessing sufficient stiffness to support its own weight and maintain its shape, known as 'extrudability'. (3) Achieving 'buildability' through reaching a certain level of yield strength is critical to support successive layers without any deformation (PAOLINI et al., 2019).

This depicts the contradicting rheological requirements in concrete printing. During pumping, it requires high workability to extrude material, yet low workability and high thixotropy are needed after extrusion to ensure structural integrity (REHMAN & KIM, 2021). Further exploration of the rheological behaviors of concrete as a printing material will be detailed in Section 2.2.

Various strategies in extrusion method have been applied, each requiring different constraints and generates distinct printing results. One common strategy is the "Infinite Brick Extrusion" that requires material with high initial yield stress and low thixotropy. This strategy typically results in layer cross-sections that match the nozzle dimensions, limiting flexibility in choosing filament dimensions. An alternative method known as the "Free-Flow Deposition" is performed by depositing printing material with lower initial yield stress from a height larger than the intended layer height. As a result, the layer height is determined by the combination of yield stress and gravity, resulting in restricting control over the final shape. Finally, the "Layer Pressing Strategy", as the focused strategy for this study, offers improved geometric control by adjusting printing parameters such as robot speed, extrusion rate, and nozzle height. With this strategy, the printing nozzle is set at specific height during extrusion, causing to press the extruded material and forms the desired filament height and width (CARNEAU et al., 2022).

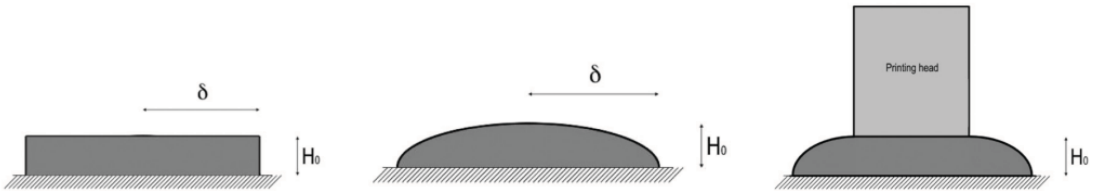

Figure 2.3: Different Techniques of Extrusion Method. Left: Infinite Brick Extrusion, Middle: Free-Flow Deposition, Right: Layer Pressing Strategy (CARNEAU et al., 2022)

2.1.2 Printing Machine and Control

AM Machinery

A key aspect to consider for construction strategy is the circumstances of the existing site. A common approach utilizes the gantry system, which features a fixed framework that provides support and mechanical guidance for the device. This stationary system allows the 3D printer to extrude paths over longer pathways due to its broad span. This system generally has fewer Degrees of Freedoms (DOFs) in comparison to industrial robot arm systems; therefore is typically more restricted in creating complex geometries and

Figure 2.4: On-site printing with a gantry system (F. P. Bos et al., 2022)

overhangs (Keating et al., 2017). It may impose limitations on confined construction sites due to the required large size of the configurations relative to the size of the built structure. Additionally, it requires long material supply distances, and extensive effort for transport and assembly (Cai, 2018).

In contrast, industrial robots, generally employed for the extrusion method, offers an alternative approach. Arm-based systems provide a higher level of kinematic flexibility, offering the possibility to create complex geometries. In cases such as deploying in a stationary position, a limitation is its restricted reach (F. P. Bos et al., 2022). For instance, industrial robot manufacturers, such as KUKA, provide robots with a typical maximum reach of approximately 3 meters in length, with a rotational range that confines construction within its semi-spherical workspace (KUKA, 2021). Nevertheless, this constraint can be mitigated through utilizing rail tracks to extend their operational reach (F. P. Bos et al., 2022).

Printing Parameters

Precise control over various printing parameters is crucial for achieving optimal results. As discussed by Carneau et al. (2022), this is particularly analyzed for the layer pressing strategy, which investigates the effect of each printing parameters to ensure a regulated printing process. The essential printing parameters are outlined in Table 2.1.

Table 2.1: Printing Parameters in Extrusion Method

Category	Parameter	Notation	Unit
Kinematic	Robot speed	Vr	mm/s
	Extrusion speed	Ve	mm/s
Geometric	Layer height	H	mm
	Layer width	B	mm
	Nozzle diameter	D	mm
Material	Initial dynamic yield stress	$\tau_{D,0}$	Pa
	Initial static yield stress	$\tau_{S,0}$	Pa
	Re-flocculation rate	R_{thix}	Pa/s
	Structuration rate	A_{thix}	Pa/s
	Density	ρg	N/m^3
Process	Extrusion force	F	N
	Inter-layer time	Δt	s

Machine Control

The initiation of the printing process in digital manufacturing systems requires advanced machine control mechanisms. These mechanisms execute a series of commands for the printing apparatus, converting digital numerical data into precise movements along its coordinate axes. In Digital Manufacturing Methods, this information typically originates from geometric representations, such as Computer Aided Design (CAD) models, where 3D geometries are derived into 2D representation consisting of pathways for fabrication. Subsequently, print path representations are transformed into machine control codes. Most Computer Aided Manufacturing (CAM) systems employ the common standard Computer Numerical Control (CNC) protocol, which relies on G-Code. G-Code comprises command sets that specify Cartesian coordinates and velocity parameters for execution. It should be noted, however, that this may vary depending on specific manufacturer that might be constrained with vendor-specific languages (SLEPICKA et al., 2021).

2.1.3 Construction Strategy

Both on-site and off-site construction present distinct benefits and drawbacks that require critical consideration. The construction strategy is influenced by the environmental conditions of the site, including factors such as ground stability, sufficient workspace, and the presence of extreme weather conditions. These factors impact the selection of construction techniques for creating safe and functional structures (KEATING et al., 2017). In an on-site construction, one key consideration involves ensuring the quality of the printed results amidst varying external environmental conditions. Fluctuations in temperature and humidity can influence the curing process, imposing challenges to accurately predict the

optimal open time for achieving desired interlayer bonding strength. Various measures can be implemented to artificially regulate environmental conditions; for instance, deploying a water mist system to control humidity levels or using protective foil to prevent early drying and shrinkage. (F. P. Bos et al., 2022). However, the effectiveness of these approaches remains subject to further evaluation, as it still lacks in data to compare its efficacy.

Conversely, off-site fabrication offers advantages in terms of managing the curing process due to the stable environmental conditions. Despite these benefits, the logistical, environmental, and financial implications for transporting printed components to the construction site require careful consideration. Additionally, while off-site fabrication is limited to producing assembly-based components, this approach sets constraints in fabricating complex geometries in virtue of maintaining structural stability (Haar et al., 2023).

The choice between on-site and off-site construction is not rigidly confined to only one of either approach. A hybrid approach, integrating both methodologies, presents a feasible option that can be tailored to the specific circumstances of the site, environmental conditions, machinery requirements, and design constraints.

2.2 Analysis of Rheological and Printing Parameters

To fully achieve a controlled and successful 3DCP, it is essential to recognize the unique behaviors exhibited by concrete printing materials at each stage of the building process. The rheological properties of these materials are crucial in shaping the printing process and result. These properties significantly influence the material's capacity to resist deformation from its self-weight, the weight of subsequent layers, and induced stress from the printing nozzle. Typically, failures in 3DCP are evident through two primary mechanisms: material and stability failure. Material failure, or plastic collapse, occurs when the strength threshold of the material is exceeded, resulting in fractures or uncontrolled deformation during printing. Stability failure, or elastic buckling, arises when the structure is not capable of maintaining equilibrium against forces post-printing due to a loss of geometrical stability.

In response to these challenges, numerous analytical models have been presented to integrate the analysis of rheological properties with printing parameters to enhance control over geometry and stability. For example, Carneau et al. (2022) proposed boundary conditions for controlled layer pressing extrusion that take into account geometric, kinematic, and material parameters. This model maps out various printing regimes and their failure modes at the scale of a single layer. It measures furthermore the pressing stress on sub-layers to ensure the buildability of the structure. Additionally, Kruger, Zeranka, and Zijl (2019) introduced an analytical model to quantify the buildability of 3D printed concrete structures based on physical nonlinearity, specifically plastic yielding. Employing the Mohr-Coulomb failure criterion, the model provides a conservative lower bound estimation of the maximum number of layers achievable, dependent on the rheology of the material.

This section systematically outlines the rheological events, printing conditions, and failure criterion relevant to each phase of the printing process: pumpability, extrudability, geometric conformity, and buildability.

2.2.1 Pumpability and Extrudability

Pumpability is characterized by the ability of the printed material to be transported through pipelines under pressure. Common practices to transport concrete utilizes external pumps such as progressive cavity pumps, positive displacement pumps, or ram extruders. As a Bingham fluid, concrete exhibits solid behavior under lower shear stresses and viscous behavior under high stresses. It requires thereupon external stress to modify its consistency to a more fluid state (REHMAN & KIM, 2021).

The dynamic yield stress, that is defined as the minimum stress necessary for inducing flow from its resting state, can be quantified under the following Bingham model's equation (MIRANDA et al., 2023):

$$\tau = \tau_0 + \mu\gamma \tag{2.1}$$

Where τ represents the shear stress (Pa), τ_0 the yield stress (Pa), γ as the shear rate (s^{-1}), and μ the plastic viscosity. The initial yield stress (τ_0) describes the minimum shear stress needed to initiate concrete flow. Below the threshold of the yield stress (τ_0), the material maintains in its solid state. Furthermore, viewing concrete as a hypothetical fluid composed of infinite layers, viscosity (μ) can be conceptualized as the resistance between these infinite layers. Higher viscosity restricts the material's flowability, significantly affecting the ease of its movement.

Extrudability measures the capacity of the material to pass through the nozzle without breakage, thereby creates a continuous filament. The initial yield stress at the nozzle exit is particularly critical; it not only determines the minimum threshold to induce flow, but also ensures that the material can withstand deformation under nozzle pressure, essential for maintaining structural integrity during printing. As WANGLER et al. (2022) suggests, the recommended yield stress for printable concrete to achieve stability ranges from 100 Pa to 10 kPa.

There are several methods that have been employed to measure yield stress. One method known as the slugs test method is used to determine the initial yield stress at the nozzle by observing gravity induced flow at the nozzle exit, which forms a slug-like shape at the onset of flow (DUCOULOMBIER et al., 2020). The yield stress at the nozzle level can be calculated based on the average mass of multiple slug drops under the following equation:

$$\tau_c = \frac{g.m_s}{\sqrt{3}.s} \tag{2.2}$$

Where g defines the gravity, m_s the mass of the slug, $\sqrt{3}$ from the Von Mises plasticity criterion, and s as the nozzle section.

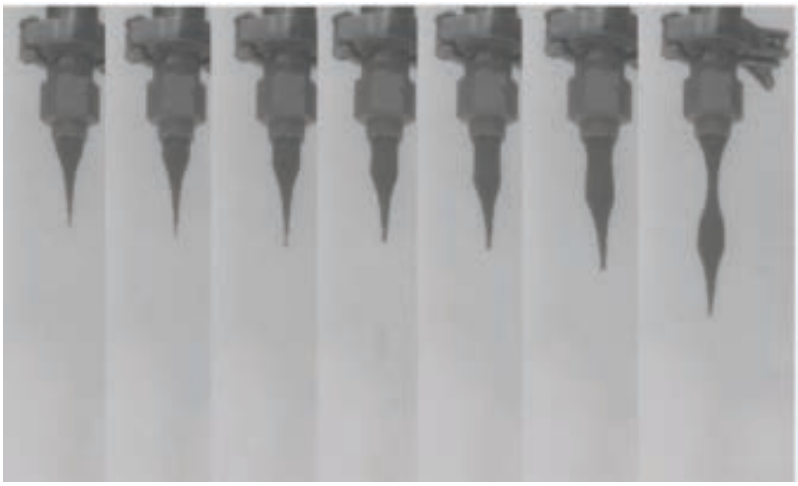

Figure 2.5: Printed Concrete Slugs at Nozzle Exit (DUCOULOMBIER et al., 2020)

The downside of the slug test method is that it is not compatible to stiffer consistencies. As the method aims to deposit slugs, on stiffer materials, it would only cause breakage in deposition. An alternative method is the slow penetration method involving a conical tip to submerge into the concrete at a slow rate to measure resistance force which is then used to calculate the yield stress. It is considered as a reliable method to measure continuous development of yield stress which also allows obtaining the structural build-up rate, thixotropy, cohesion and flow behavior (REITER et al., 2022).

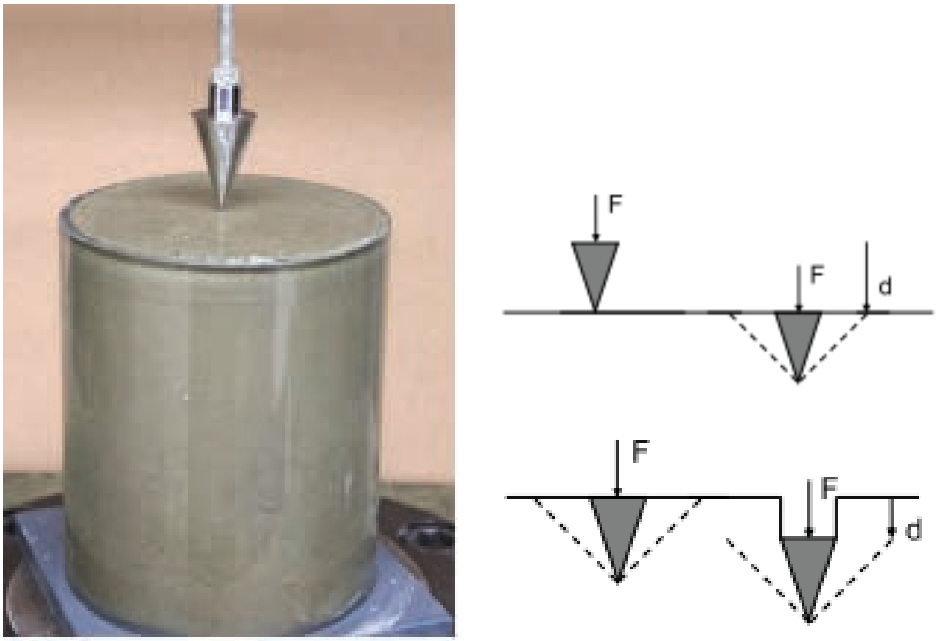

(a) (b)

Figure 2.6: (a) Sample concrete container and penetration tip, (b) Starting point of penetration test with increasing depth d (REITER et al., 2022)

Another aspect is the open time that represents the duration in which the material remains extrudable. Fresh concrete possesses a rapid thixotropic (reversible) behavior that is capable to flocculate (clump together) or deflocculate (disperse) based on presence or absence of applied shear force. When the external shear force is removed, in other

words, when the material is at resting state, flocculation starts to occur, resulting in an activation of the static yield stress. There is only a certain period of short time when the thixotropic effect (reversible) is still dominant. Once this time limit has surpassed, the material enters an irreversible state where hydration process is more dominant. in which the static yield stress of fresh concrete increases- an event known as structuration. The structuration rate (A_{thix}) defines the increase rate of static yield stress with time, whereas the rapid re-flocculation rate (R_{thix}) defines the reversible particle flocculation process which occurs in the first few hundred seconds after the removal of the applied shear force (KRUGER, ZERANKA, & ZIJL, 2019). As a rule of thumb, the thixotropy of the material can be modeled not more than 30 minutes, in which the irreversible evolution of the concrete can be neglected (ROUSSEL, 2006).

2.2.2 Geometric Conformity

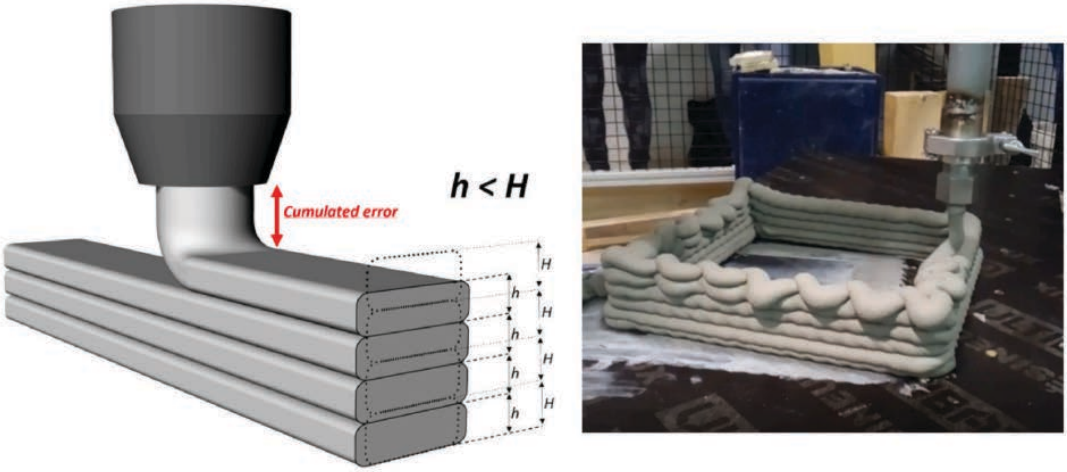

Figure 2.7: Result of overflow deposition due to higher level of nozzle printing (CARNEAU et al., 2022)

A further aspect that requires attention after deposition is the geometric conformity of the printed shape. Both material properties and printing parameters significantly impact the final form of the structure. A phenomenon called "flow-out" occurs when the target height exceeds the capacity of the yield stress to maintain the material's form. The boundary condition for this type of failure can be expressed according to the Von Mises failure criterion:

$$\tau_0 = \frac{\rho.g.h_L}{\sqrt{3}} \tag{2.3}$$

Where ρ defines the volumetric mass, g the gravitational constant, and h_L the layer height or printing height. Failure to meet this condition can result in deformations, leading to a decrease in the intended height. This accumulating decrease from deformation can result in poor control over the deposition process. If the height of the printing nozzle is set too high, it can result it coiling patterns, as demonstrated in Figure 2.7.

In addition, longitudinal tearing can occur if the printing speed (V_r) is larger than the extrusion speed (V_e). This condition is described with a dimensionless **speed parameter** V^* defined by CARNEAU et al. (2022), where $V^* = V_r/V_e$. Thus, high value of V^*, such as with value of 5,6 as depicted in Figure 2.8, may lead to inconsistent division of material deposition.

Figure 2.8: Longitudinal tearing at higher speed rate (V^*) above the bounding condition (CARNEAU et al., 2022)

2.2.3 Buildability

Buildability describes the ability of sequentially printed concrete to reach a specific height without significant deformation or collapse of the layers. Such factors that mold the buildability behavior are the mechanical properties of the printing material, the curing rate, the geometrical features of the printed structure, and the process parameters. Structural failure that affect buildability in 3DCP include elastic buckling and plastic collapse. Elastic buckling occurs when a structure deforms laterally under compressive stress, leading to a sideways deflection. It is influenced by the stiffness of the material, curing rate and the geometric characteristics of the printed structure. Whereas, the plastic collapse is characterized by the material yielding under stress, leading to permanent deformation and structural failure.

Material's Structural Build-Up

Understanding the thixotropy model of a material is crucial for targeting material resistance to failure. ROUSSEL et al. (2012) proposed a model that describes the evolution of static yield stress τ_s linearly over time (Eq. 2.4). This model is primarily accounted for the **structuration rate** (A_{thix}) particularly based on colloidal interactions and Calcium Silicate Hydrate (CSH) nucleation.

$$\tau_t = \tau_0 + A_{thix}.t \tag{2.4}$$

The linear model considers a constant rate of hydration heat. However, this linear increase in yield stress persists only up to approximately 60 minutes. After this period, the rate of yield stress increase accelerates due to the formation of hydration products. PERROT et al. (2016) introduced an exponential yield stress evolution model that characterizes a smooth transition from the initial linear increase to an exponential progression (Eq. 2.5). This model includes a characteristic time, t_c which is adjusted to align with experimental values.

$$\tau_t = \tau_0 + A_{thix}.t_c(e^{trest/t_c} - 1) \tag{2.5}$$

Furthermore, KRUGER, ZERANKA, and ZIJL (2019) proposed a bi-linear model (Figure 2.9) extending Roussel's model that is characterized by the evolution of two distinct linear phases: (1) an initial rapid increase: occurring in the first few hundred seconds, this phase is characterized by re-flocculation R_{thix} due to attractive forces between the interparticles, influencing the growth of the dynamic yield strength τ_D. (2) A long-term increase: this phase is driven through hydration in which the static yield stress τ_s is restored after re-flocculation, indicating structuration A_{thix}.

Eq. 2.6 depicts the growth of static yield stress that occurs immediately after the material has been sheared (i.e., during pumping or extrusion). Where Eq. 2.7 maps the structuration phase, in which it ensures that the material gains additional strength and stability over time. The variable t_{rf} serves as the transition point between the two phases of the bi-linear model.

$$\tau_s(t) = \tau_{D,i} + R_{thix}.t \tag{2.6}$$

$$\tau_s(t) = \tau_{S,i} + A_{thix}.(t - t_{rf}) \tag{2.7}$$

$$t_{rf} = \frac{\tau_{S,i} - \tau_{D,i}}{R_{thix}} \tag{2.8}$$

Despite acknowledging the exponential growth of the yield stress, this model focuses more on the re-flocculation R_{thix} process and the early phases of structural build up, making it applicable for 3D printable materials where immediate structural recovery after deposition is critical, followed by a sustained increase in strength and stiffness over a certain period of time.

Building Rate

In 3DCP, the building rate is one of a critical factor that determines stability and buildability of the printed structure. It is defined as the rate at which a structure is printed, influenced by printing and geometric parameters. This factor considers the influence of the normal stress due to the upper layers applied to the bottom layers, along with the time-dependent

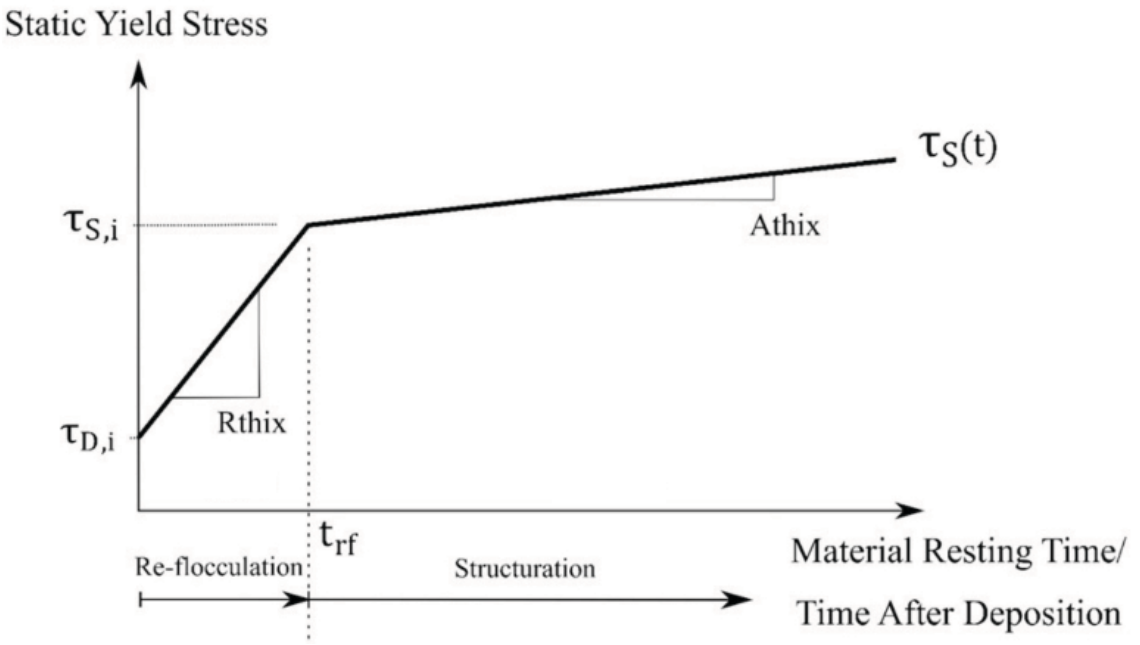

Figure 2.9: Bi-Linear model of static yield stress evolution by both re-flocculation and structuration thixotropy mechanisms (KRUGER, ZERANKA, & ZIJL, 2019)

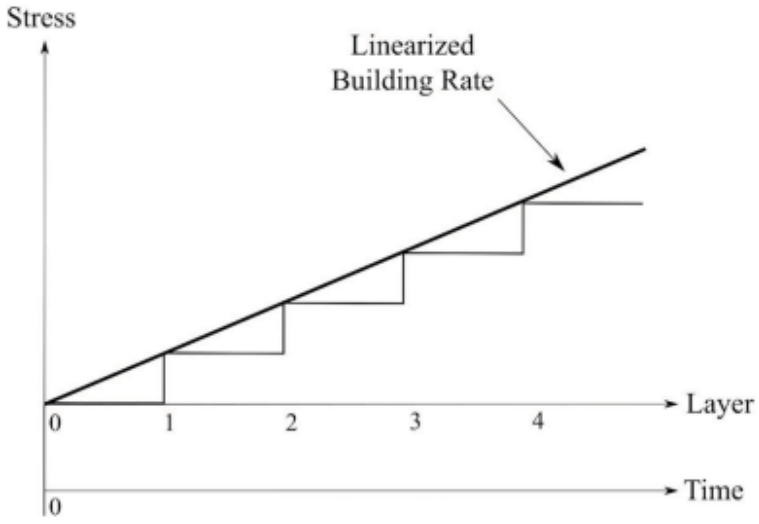

Figure 2.10: Linearized Building Rate of a Uniform Layer Geometry (KRUGER, ZERANKA, & van ZIJL, 2019)

strength development (KRUGER, ZERANKA, & van ZIJL, 2019). Assuming uniform geometry across each layer, the stress from each layer remains constant, resulting in a linearized building rate. A higher building rate leads to a rapid increase in stress, whereas a slower rate allows more time for the structure to gain strength before deposition of new layers. The total normal stress in relative to the number of layer (N_L) towards the critical bottom layer can be expressed in Eq. 2.9.

$$\sigma(N_L) = \rho.g.h_L.N_L \tag{2.9}$$

Failure Modes – Plastic Failure

Understanding the limitations of printed structures and analyzing them to obtain optimized printing parameters is key to achieve better stability and load-bearing capacity. As mentioned briefly in Section 2.2.3, main failure modes in 3DCP are classified in two types: elastic buckling and plastic failure. Elastic buckling occurs when the printed structure deforms significantly due to compressive stresses exceeding the critical buckling load, which is mainly influenced by factors such as geometry and material properties. It is characterized by significant lateral deformations. On the other hand, plastic failure occurs when the material experience irreversible deformation due to stresses surpassing its yield strength, indicated by vertical displacements and surpassing lateral ones.

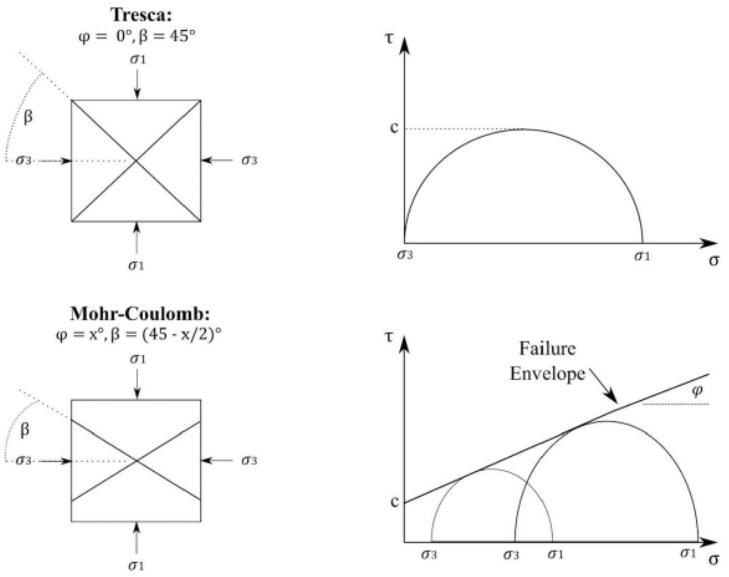

Figure 2.11: Tresca, Mohr-Coulomb and Rankine behavior illustrated as infinitesimal elements and Mohr circles (KRUGER, ZERANKA, & van ZIJL, 2019)

Addressing these failure modes, Kruger developed a lower-bound analytical model that predicts buildability performance by considering the thixotropic behavior of the concrete and the plastic yield of the structure. Although the model simplifies the approach by not accounting for geometric nonlinearity (i.e., elastic buckling), it provides a conservative estimate of material performance (bilinear structural growth) and applies the failure mech-

anism based on the Mohr-Coulomb failure criterion. This criterion accounts for materials that exhibit both cohesive and frictional properties. The criterion is given by:

$$\tau = c + \sigma.tan(\phi) \tag{2.10}$$

where τ defines the shear stress at failure, c cohesion of the material, σ normal stress, and ϕ the angle of internal friction.

The shear strength of fresh concrete, immediately after mixing, is primarily due to interparticle friction. As the concrete hardens, cohesion develops from early hydration products that bind the constituents together. Materials with high workability generally exhibit smaller internal friction angles, whereas those with low workability display larger friction angles. In cases where the friction angle equals zero and $\sigma_3 = 0$ due to uniaxial stress state, the Mohr-Coulomb criterion simplifies to the Tresca failure criterion-the lower bound of the criterion (Figure 2.11), where the maximum shear stress is:

$$\tau = \frac{\sigma_1}{2} \tag{2.11}$$

It is however crucial to consider the effects of confinement, as it directly affect the transverse stress. The aspect ratio (height to width) of the filament layers influences the apparent strength due to confinement. In the uniaxial stress state, σ_1 equals the applied normal stress and σ_3 equals zero (Tresca failure). As the aspect ratio decreases, a triaxial state of stress exists due to confinement which increases the material's interparticle friction and capacity against shear failure. To address the confinement effects, strength correction factor F_{AR} is utilized. Thus, the relationship between normal and shear stress incorporating the strength correction factor is given:

$$\tau = \frac{\sigma}{2.F_{AR}} \tag{2.12}$$

The plastic yield of the affected layers occurs when the building rate exceeds the time-dependent material shear strength. Thereby the bulding rate, caused by the applied normal stress, is expressed in terms of shear stress:

$$\tau(N_L) = \frac{\rho.g.H_L.N_L}{2.F_{AR}}, N_L \in \mathbb{R} \tag{2.13}$$

This must be taken into account that the provided buildability analysis implies material properties such as cohesion, internal friction angle, and Poisson ratio are assumed at its minimal state and adjusted by strength correction factor. Furthermore, it considers vertically printed structures; therefore non-vertical objects with more geometrical freedom may require further considerations such as eccentricity and contact surface of successive layers, thus a numerical approach may be required.

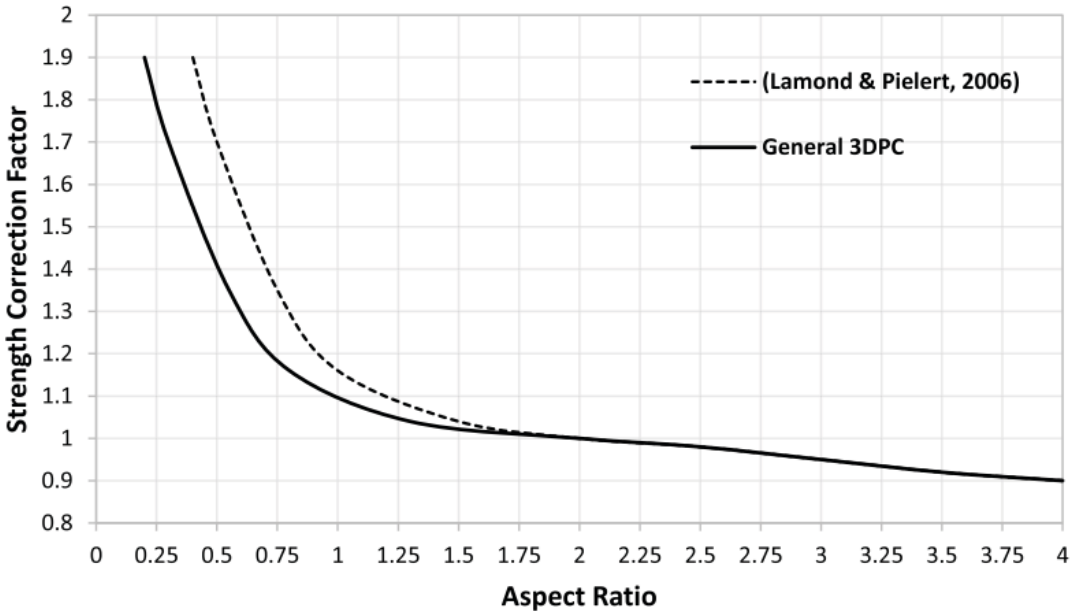

Figure 2.12: Strength correction factors for various aspect ratios (KRUGER, ZERANKA, & ZIJL, 2019)

2.2.4 Printable Mix Designs

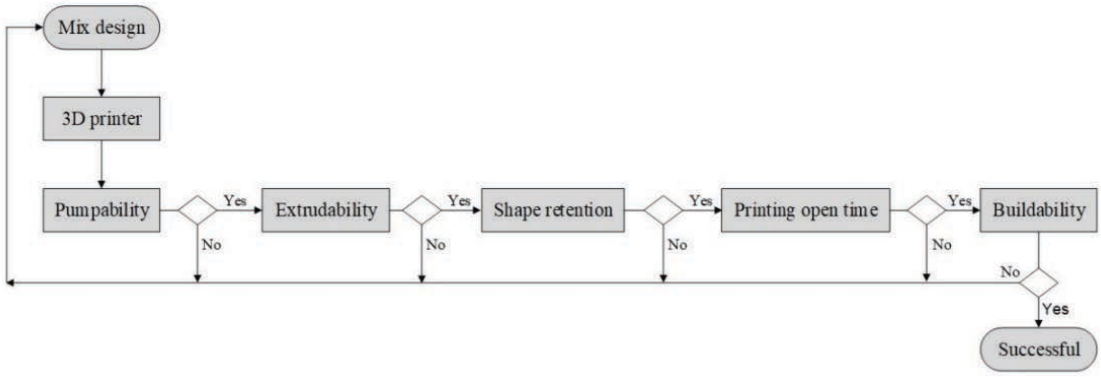

Figure 2.13: Iterative Process to Ensure Printable Concrete Mix (REHMAN & KIM, 2021)

The design of printable concrete mixes involves a series of considerations to meet specific requirements essential for 3D printing processes, as outlined in previous subsections. According to REHMAN and KIM (2021), concrete mix design should undergo sequential evaluations, ensuring that each of the requirements is systematically met. In general, printable concrete mixes are characterized by a low dynamic yield stress to facilitate pumping and extrusion, while also possessing high thixotropic behavior post-extrusion to significantly enhance the static yield stress.

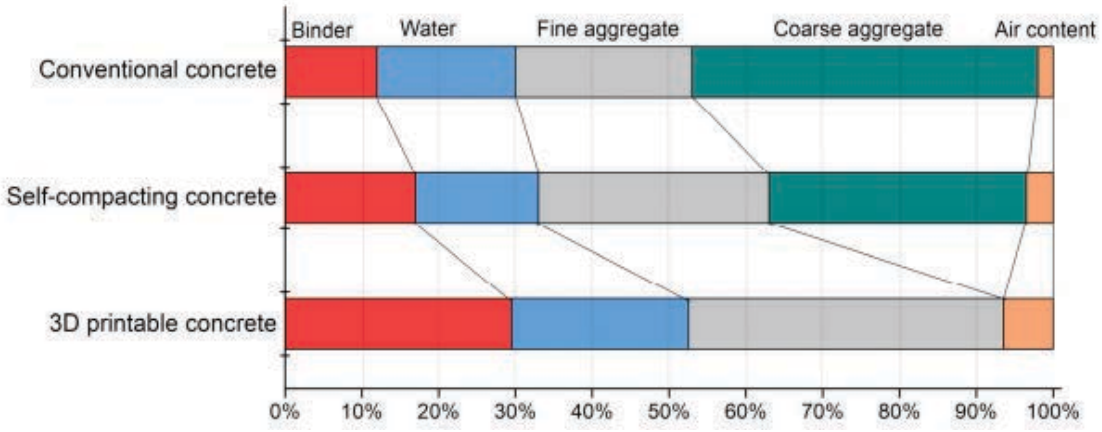

Figure 2.14: Comparison of material composition used in conventional concrete, self-compacting concrete, and 3D-printable concrete (REHMAN & KIM, 2021)

To prevent blockages in the printing apparatus, the use of coarse aggregates is typically omitted in printable concrete mixes. Instead, these mixes incorporate fine aggregates with particle sizes commonly below 2 mm. Additionally, printable mix compositions are designed to be stiff and present higher green strength to sustain its self-weight and maintain the integrity of successive layers. As such, a lower water-binder ratio and higher binder-sand ratio are recommended. The mix proportions of a water-binder ratio should lie within the span of 0.30-0.40, as for sand-binder ratio varies between 1.2-2.0 (REHMAN & KIM, 2021).

Recent research has explored integrating of ultra-high-performance fibers into concrete mixes to enhance material reinforcement. However, the addition of fibers can reduce workability, presenting challenges during the pumping and extrusion phases, necessitating further investigations (ZHU et al., 2019). An alternative approach to enhance interlayer bond strength involves incorporating pastes. MARCHMENT et al. (2019) investigated various paste mixes to assess their impact on compressive strength and interlayer bond strength. One such formulation includes a polymer-based retarder aimed to minimize the heat of hydration effects, thereby slowing the drying of the surface layers. Additionally, the use of polycarbonate ether-based superplasticizers promotes greater cement particle dispersion, enhancing workability and facilitating interlayer bonding.

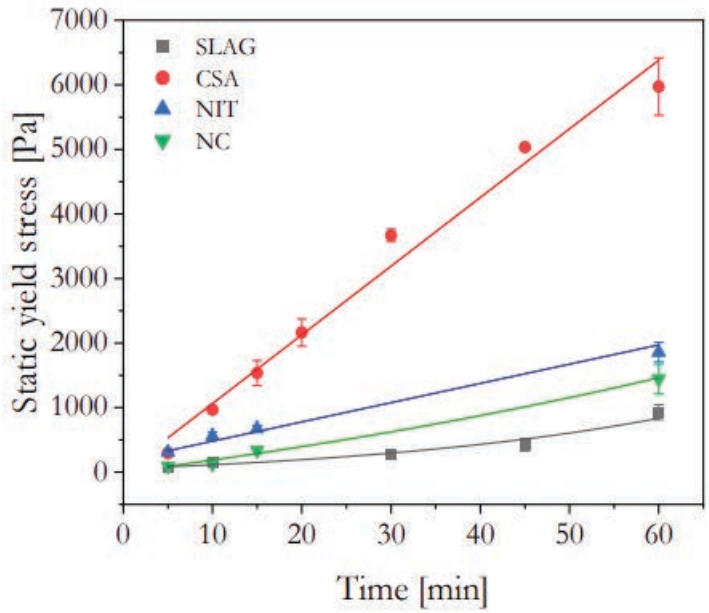

Figure 2.15: Comparison of static yield stress growth between reference cement without additives (SLAG), addition of calcium sulfoaminate (CSA), calcium nitrate (NIT), and nano clay (NC) (MIRANDA et al., 2023)

The study by MIRANDA et al. (2023) investigated the structuration growth of printable concrete, emphasizing the challenges in balancing the reversible process of flocculation with the irreversible process of hydration, both of which are essential for maintaining the shape and stability of the material during 3D printing. This research utilized calcium sulfoaminate (CSA) as a partial substitute for Portland cement, due to its accelerated setting properties. Furthermore, the addition of admixtures such as calcium nitrate (NIT) and nano clay (NC) was employed to control the temporal state of the cement. Calcium nitrate, serving as an antifreeze agent, accelerates the setting process, enhances long-term strength, and inhibits corrosion. Meanwhile, the incorporation of a small amount of nano clay increases thixotropy, promoting a stable microstructure with a higher viscosity at rest.

2.3 Building Information Modelling (BIM)

BIM at its essence describes a digital representation of three-dimensional model of building components that not only delivers its geometry model but also contains semantic information. The establishment of BIM is based on the idea of using a digital building model consistently throughout a building's entire life-cycle. It is a working method that integrates different construction sectors as one system, facilitating cooperative work among project members (BORRMANN et al., 2018)

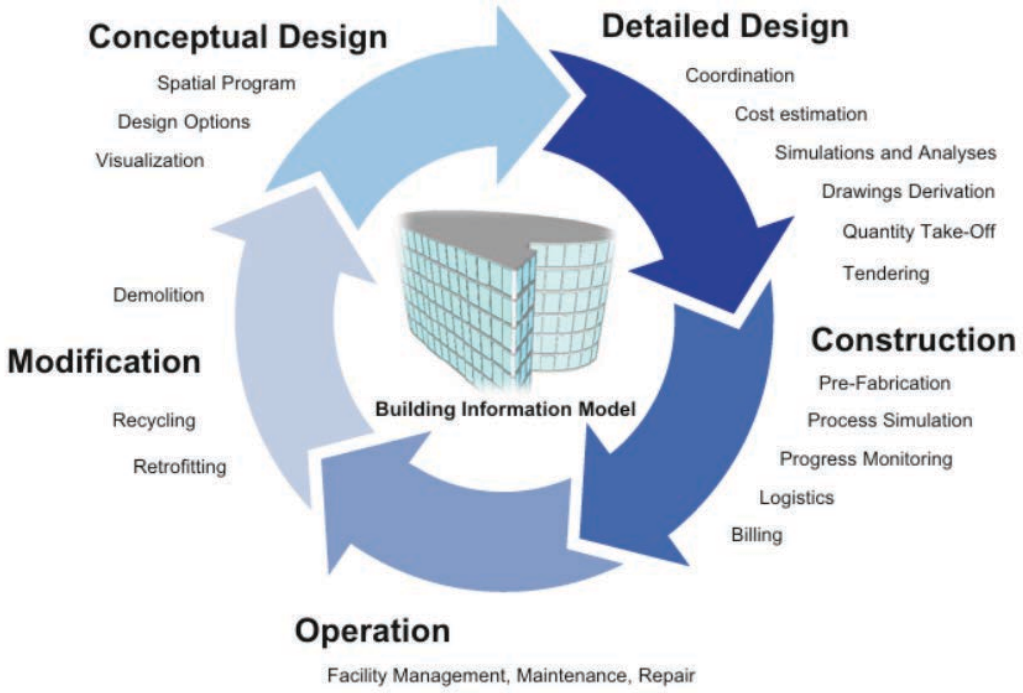

Figure 2.16: Continuous use of BIM throughout the lifecycle of a building (BORRMANN et al., 2018)

Building elements in object-oriented modeling are embedded with semantic information such as definitions, attributes, relationships, and interactions with other elements. According to EASTMAN (2008), parametric BIM Objects are characterized as follows: (1) Object with geometric definitions, (2) No redundancy or inconsistencies in geometry representations; thereby, elimintating separate 2D and 3D models in favor of an integrated model defined with relationships, (3) Objects represented in hierarchical levels, to define the relation between components (4) Its modification automatically updates associated geometries, (5) Capability to identify violations of object feasibility (6) Objects that have the ability to integrate and exchange sets of attributes.

In addition, the purpose of BIM serves to sustain a continuous, iterative process of managing building data throughout its life-cycle (see Figure 2.16). Starting from the design development phase, where detailed 3D models, simulations, compliance checking, or quantity take-offs are generated. This provides not only detailed visualization of the building, but also allows identifying potential issues in the design and accuracy in information available for various stakeholders. Planning with BIM thereby shifts the workload

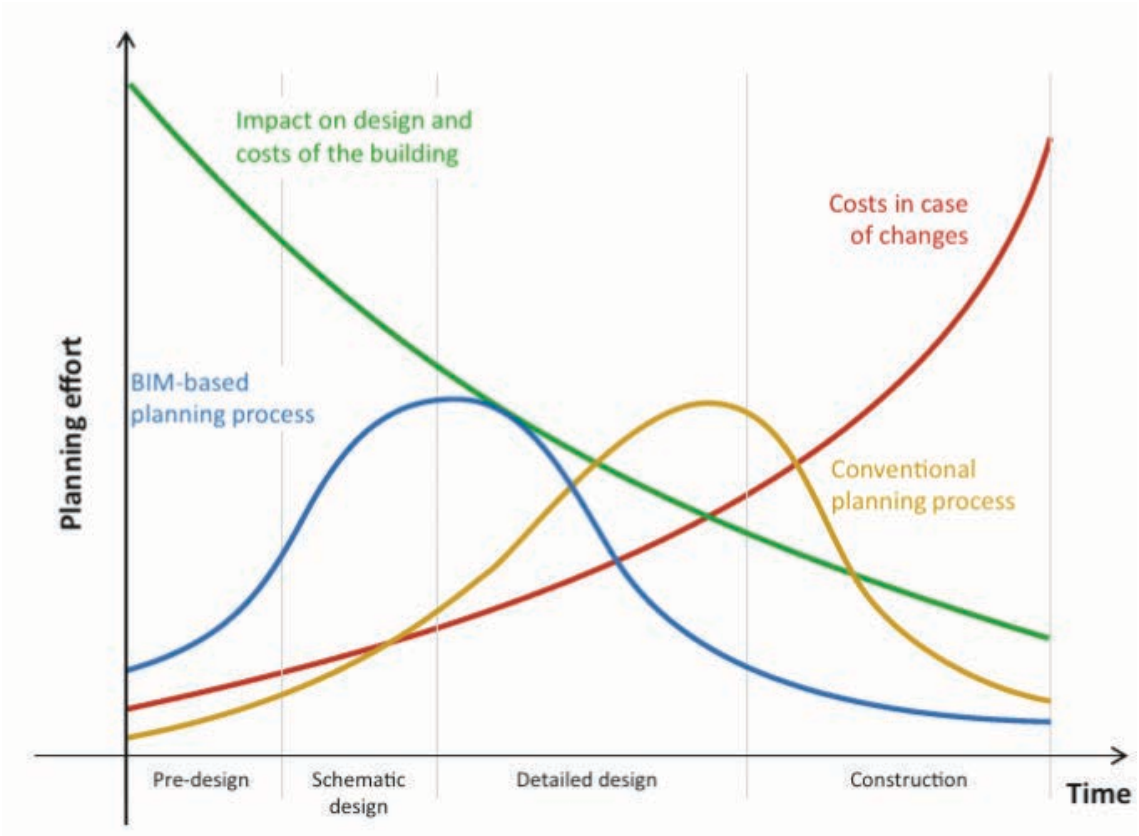

Figure 2.17: Planning effort through BIM, influencing the design, performance and cost of the resulting facility (BORRMANN et al., 2018)

to the earlier phases of planning, unlike conventional planning processes where detailed technicalities emerge in the later design phases. Furthermore, during the construction phase, information of cost and scheduled construction times can be retrieved in the BIM data, simplifying the tendering process and execution regarding construction sequence. Additionally, in the operation phase, the management and updating of information can be performed, supporting in maintenance of the building.

2.4 Semantic Web Technology and AMC Formal Knowledge

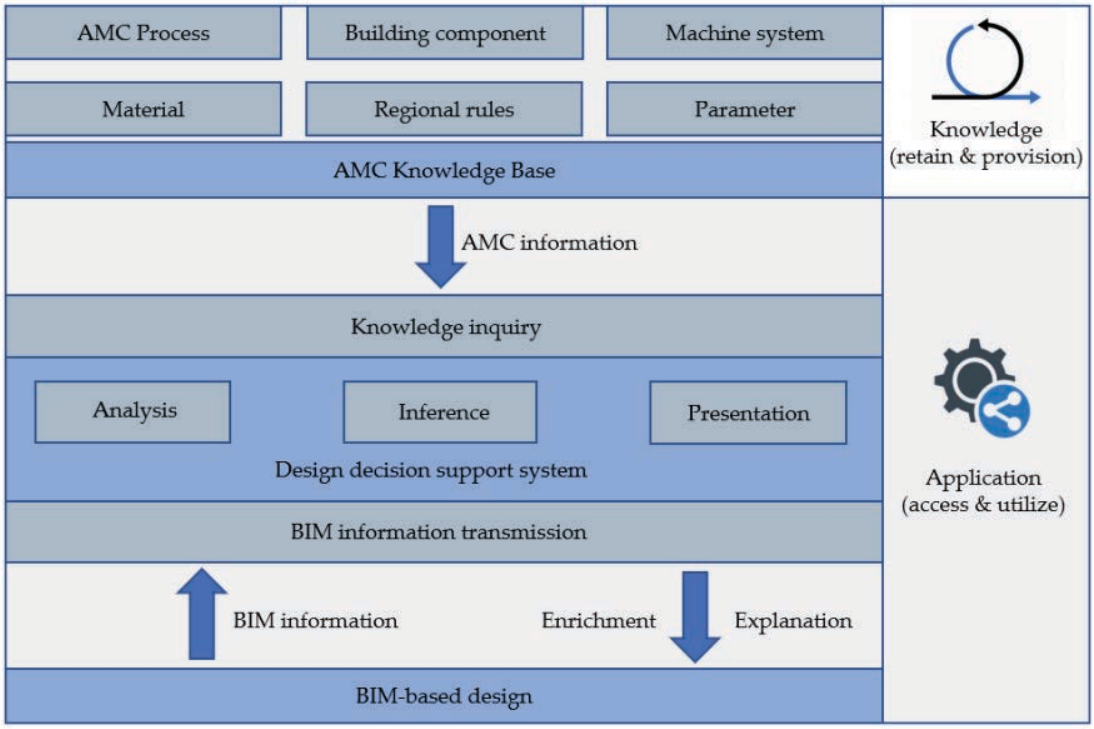

Figure 2.18: DDSS Structure for AMC (LI & PETZOLD, 2022)

Further extending the capabilities of BIM, semantic web technologies introduce advanced functionalities beneficial for the AEC industry, including interoperability, cross-domain data linking, complex querying, and logical inferences. Semantic web standards such as Resource Definition Framework (RDF) and Web Ontology Language (OWL) allow to represent knowledge that defines relationships and concepts within a domain and also combine information across domain. RDF represents graph-based data structure in form of triples (subject, predicate, object), while OWL builds upon RDF's triple model with more expressive capabilities. It facilitates the construction of detailed ontologies, which are formal representations of knowledge within a domain, encompassing a set of concepts, entities, and relationships (PAUWELS et al., 2017). Commonly misunderstood as data structures, data structures focus mainly on efficient data storage and retrieval, whereas Knowledge Representation (KR) deals with complex relationships and logical structuring of information, enabling data interpretation; thus provides meaning to data, allowing machine-based decision-making (DAVIS et al., 1993).

In the context of the AEC industry, utilizing the potential benefits of semantic web technologies to create formal knowledge can significantly support managing complex information, leading to better assessment (GURSEL DINO et al., 2009). This presents an opportunity for AMC when addressing the complexities of its methods, such as machinery requirements, logistical constraints, or structural integrity. Addressing this issue, LI et al. (2022) presents the development of an AMC knowledge base designed to bridge the gap between BIM-based design and AMC execution. This knowledge base utilizes Basic Formal Ontology

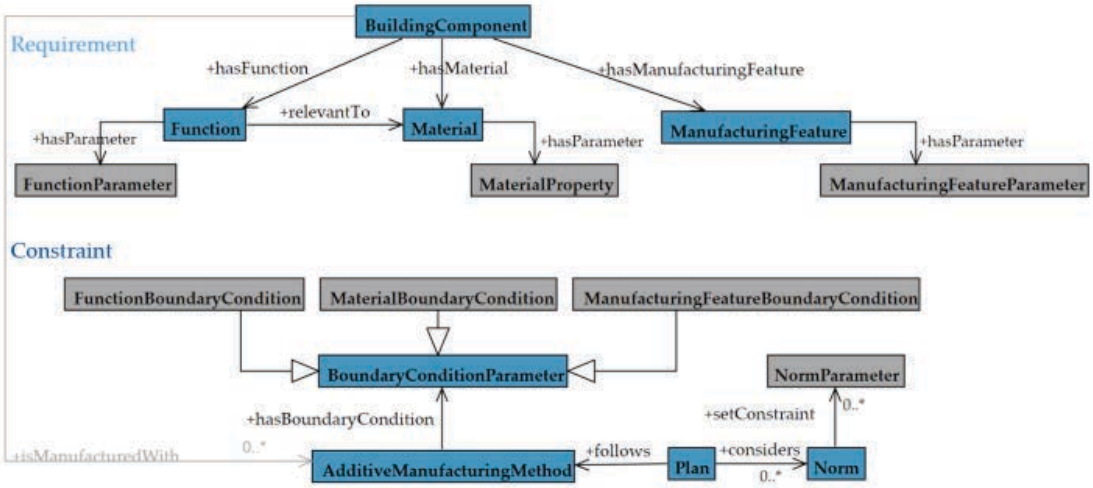

Figure 2.19: Demonstration of constraint and requirement pattern employed for AMC (Li et al., 2022)

(BFO), aligning with ISO standards, for its top-level ontology to provide a framework for integrating various domain-specific ontologies. In the intermediate layer, the Industrial Ontologies Foundry (IOF) is used that focuses on manufacturing domains, encompassing design, supply chain, production, maintenance, and life-cycle management. Furthermore, Web Ontology Language Description Logic (OWL2 DL) is employed to define the relationships and concepts within the knowledge base with role-based modeling patterns to neatly and consistently describe specifications.

Incorporating the AMC knowledge base as a foundation to the DDSS prototype, the primary goal is to offer knowledge-driven support for architects and engineers during the early phases of design. As a proof of concept, the prototype is accessible through a Revit plug-in, which retrieves geometrical and semantic information from BIM models. It utilizes feature extraction algorithms to process the data that is subsequently transferred to the DDSS portal via Remote Procedure Calls (RPC). Utilizing OWL and SPARQL, the system allows data manipulation, enabling to list, filter, and compare relevant information on AM methods, such as material properties and machine specifications.

2.5 Fabrication Information Modelling (FIM)

As BIM entails a digital model enriched with geometric and semantic information, its technology however facilitates primarily for conventional manufacturing methods, where information regarding detailed construction process is typically not required. Although manual process to convert BIM models to manufacturing data exist, it often involves multiple data format conversions through various software application, leading to risk of data loss. Thereby, FIM serves to bridge the gap between BIM and Digital Manufacturing (DM), creating a seamless digital chain from design to manufacturing in the construction industry. FIM derives BIM models automatically as its foundation, extracting necessary information required by applying rules and patterns to generate digital fabrication data. Furthermore, it aims to enhance interoperability through each design phase with appropriate interfaces to make data available to all operations within the planning process (SLEPICKA et al., 2021).

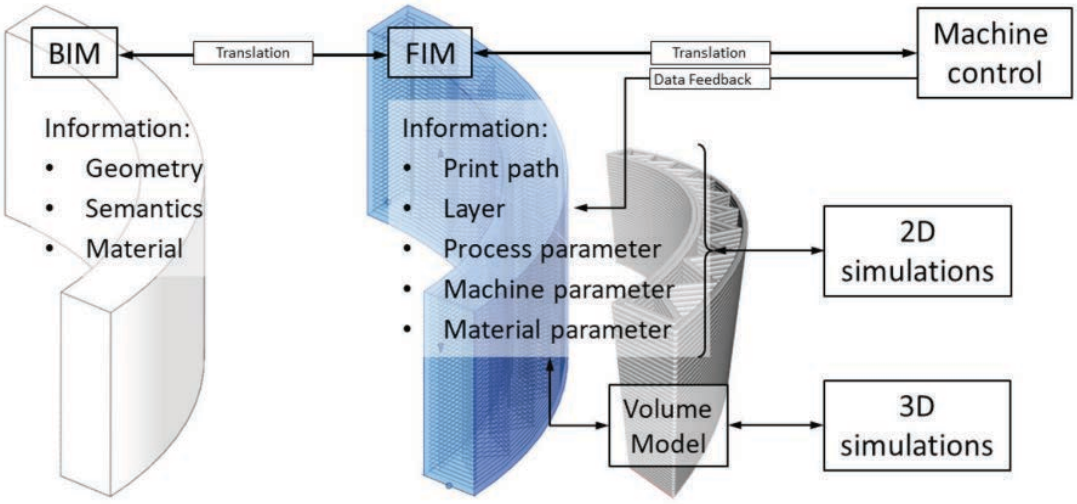

Figure 2.20: BIM and FIM Interface (SLEPICKA et al., 2022)

The FIM data is organized into three categories. Firstly, is the core information, which consists of the data that delivers the manufacturing process such as the printing path and its process information. Second category is the material distribution derived from the core information, transformed as a solid model or "as-designed" model for simulations. Lastly is the digital copy, consisting of collected data post-manufacturing, in other words "as-manufactured" model. An existing study presented by (OZTOPRAK et al., n.d.) explores the integration of FIM and Finite Cell Method (FCM), utilizing the "as-designed" model to streamline the design and analysis of AM building components, examining the mechanical and thermal performance.

2.5.1 Process Information

With the myriad of AM technologies and the complex nature of the process, performing FIM requires parameter sets to be tuned according to different AM systems that demands diverse requirements to ensure feasibility. As stated in SLEPICKA et al. (2021), these parameters are categorized in material parameters, process parameters, and machine parameters. Material parameters entail material composition and rheological properties which influence the printing process and its stability. Process parameters describe the properties that influence the manufacturing process, such as speed rate, layer dimensions, nozzle size, etc. Machine parameters include the settings within the machine systems that constrain the process parameters, such as axle speed, rotation, and acceleration. Robot systems for example have unique range of motion and limiting reach which constraints the maximum size of the design; thereby, proving the necessity to include these parameters in planning.

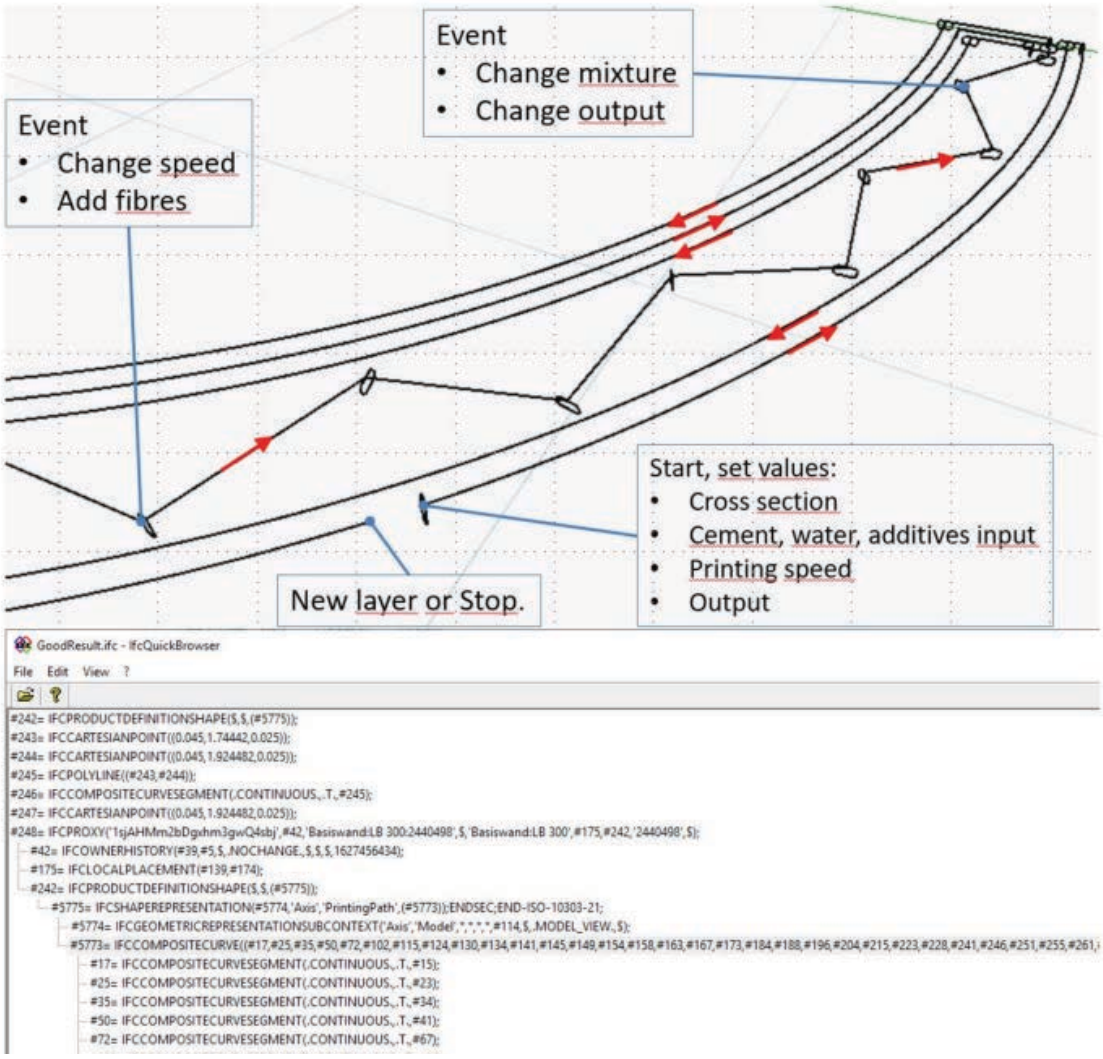

Figure 2.21: FIM model representation of one layer print path (SLEPICKA et al., 2021)

2.5.2 FIM Framework

The printing path generation is a key aspect of a FIM model, determining the movement and operation of the printing nozzle during the manufacturing process. A prototype of the FIM framework (SLEPICKA et al., 2021) utilizes Dynamo, a visual programming tool serving as an interface for the Revit API. This process begins with the slicing operation, where the 3D BIM model is divided into series of 2D slices (layers) in order to obtain a layer-by-layer format for the printing machine. Detailing the FIM model includes creating paths for the inner structure, with the ability to pre-select of various in-fill designs. The design of the printing path can be exported in an IFC data model, which its data structure is similarly compared to roadway/railway design. The geometric form of the layers is represented as curves, which in a FIM data model are denoted as `IfcCompositeCurve`, and can also be defined as `IfcLinearPositioningElement`, describing the positioning of the printing nozzle. Furthermore, the velocity profiles defined in the FIM framework refers to the printing nozzle's velocity. It is set as a non-constant parameter, which is linearly referenced as the path geometry in constraint to the defined layer time. This allows for precise control of the material flow, minimizing defects in printing.

Chapter 3

Implementation

3.1 Concept Overview

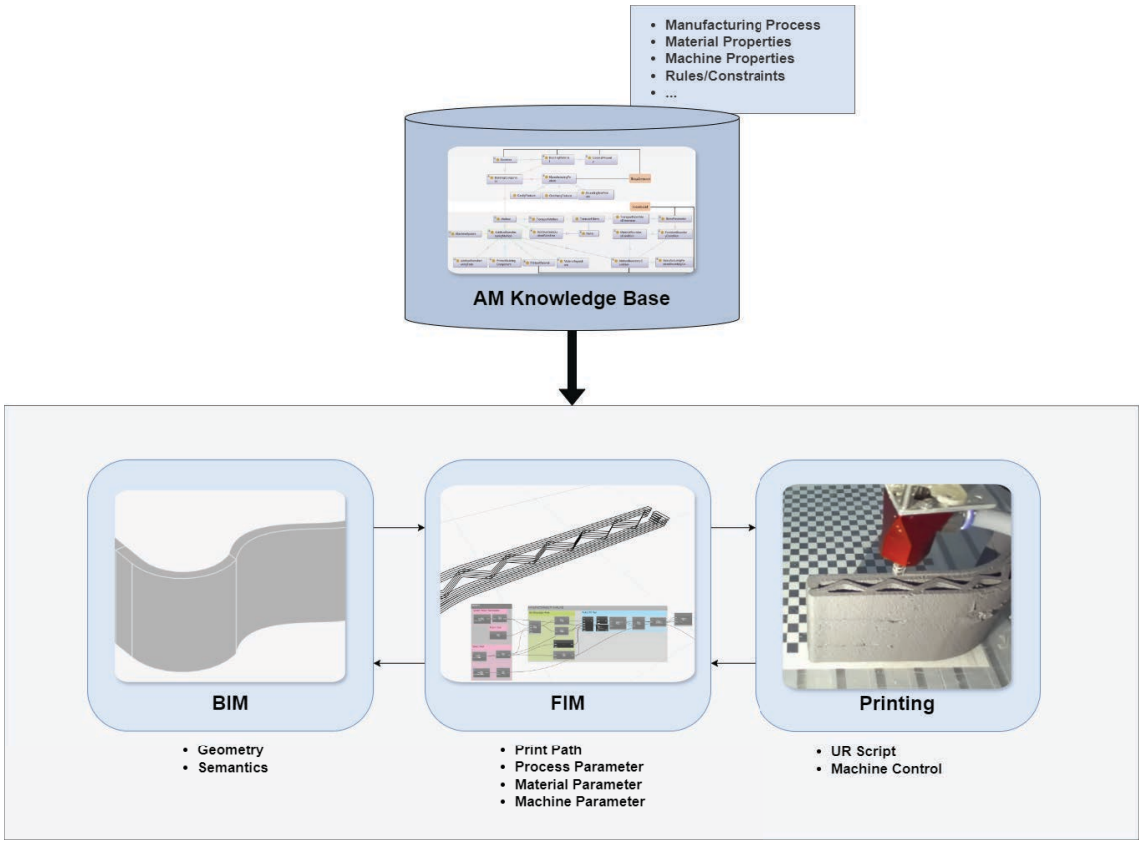

Figure 3.1: Conceptual method integrating AMC knowledge base into BIM, FIM, and printing process

Building upon the theoretical framework elaborated in Chapter 2, this chapter explores the implementation as defined in the introduction. The objective of this chapter is to develop an interconnected system between the AMC knowledge base and the FIM framework as depicted in Figure 3.1. The AMC knowledge base (Li et al., 2022) provides potential in delivering detailed information of AM methods, materials, machine systems, and constraints, which can be made available for BIM, FIM, and the printing process. The aim of this implementation is to retrieve appropriate values of process parameters under the influence of material properties to ensure extrudability, buildability, and structural integrity.

Firstly, the development of the knowledge base and its integration into the FIM framework are described. Consequently, based on the theoretical background elaborated in Chapter 2.2, applied analytical models are concluded and embedded in the FIM framework, utilizing

the information queried from the AMC ontology. Finally, a conservative manufacturability analysis is outlined to assess constraints related to the printing workspace area.

3.2 Applied Software

This study employs several software tools to support design modelling, knowledge formalization, analysis, and automation needed for .

Revit

Autodesk Revit is a software tool widely used in the AEC industry for BIM. It supports all phases and disciplines in a construction project, allowing comprehensive design, planning, and project management based on a single BIM data. Revit's features enable modeling of parameterized building objects, multidisciplinary coordination, quantity take-off, and interoperability (AUTODESK, 2024). With its capacity to incorporate both geometric and semantic information in building designs, Revit is ideal for creating sample BIM models for further analysis.

Dynamo

Dynamo for Revit is an open source visual programming platform integrated in Revit, enabling users to access Revit's Application Programming Interface (API). It allows the development of custom logic for automation, enabling the construction of complex parametric geometries and handling of repetitive tasks. Dynamo is furthermore used to extract geometric and semantic information from Revit BIM models. It also offers a library of predefined nodes for visual programming and supports textual programming in DesignScript, Python, and C#. For this study, Dynamo 2.1.0, compatible with Revit 2024, was used alongside Python 3.9.12. The Python libraries included are NumPy, Neo4j, RDFLib, and ifcopenshell.

Protegé

Protégé is an ontology editor for knowledge-based solutions, making it an appropriate tool for formalizing AM knowledge. It supports the latest OWL 2 Web Ontology Language and RDF specification from the World Wide Web Consortium (W3C). It is integrated with reasoning tools that perform consistency validation checks and infer new knowledge from existing relationships and rules.

3.3 AMC Formal Knowledge

3.3.1 Knowledge Formalization

The knowledge formalization is done based on a rework of what has been done from the paper Li et al. (2022). The formal knowledge encapsulates domain-specific information, constraints, and rules that guide both design and construction processes. Throughout the study where new information are added and adjustment occurs, the knowledge base is designed in a way that it is scalable and adaptive by incorporating continuous improvement through iterative evaluations, updating the ontology with new knowledge. It aligns with DOLCE+DnS Ultralite (DUL) to ensure consistency and extensibility, accommodating evolving requirements. The role-based pattern equipped by DUL is applied in the AMC ontology to define various entities and their relationships, allowing for the categorization of components such as building materials that can be defined as roles, and their corresponding functional properties such as material specifications as their attributes. Furthermore, it utilizes BFO to express terms of "capability" and "function" useful in the engineering domain. On a more specific note, the middle layer of the ontology aligns with IOF, where specific advantages for the manufacturing domain, such as detailed modeling of manufacturing processes and resources are described.

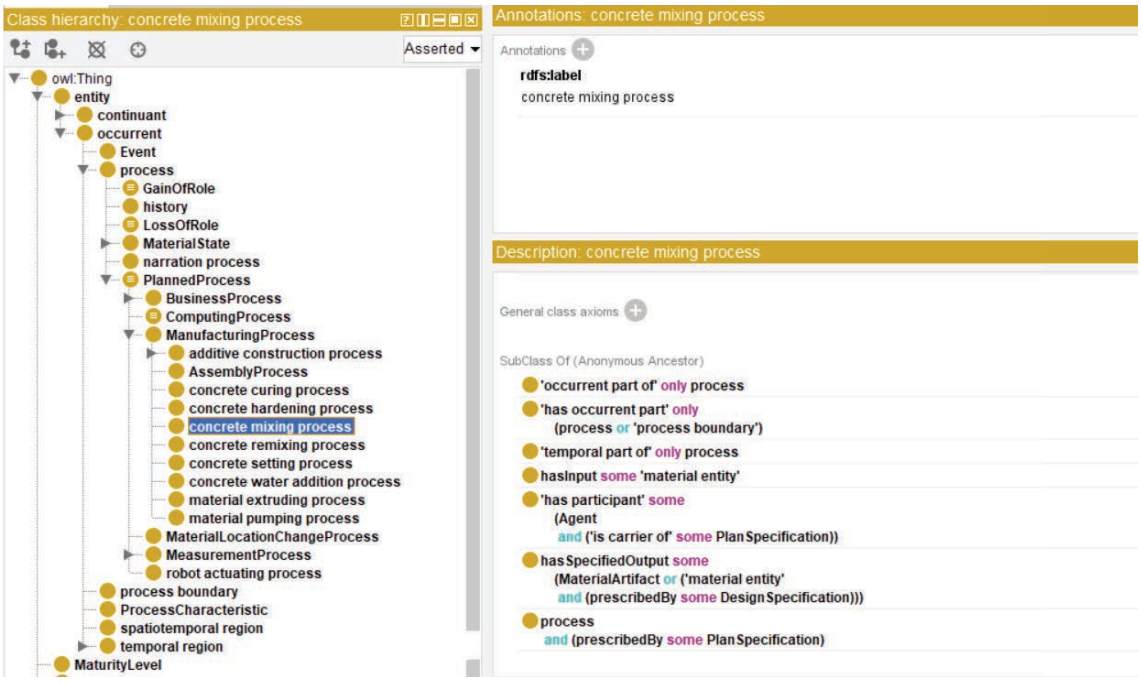

Figure 3.2: Development of AM Ontology in Protégé

Figure 3.3 depicts the snippet of the ontology, encompassing the manufacturing process. The units displayed in yellow represent the process entities within an AM process. The processes entails relations with physical components, defined as role entities, serving as the given functionality defined in the relationship (i.e., input, output) of the processes. These physical components such as material ingredients, hose pump, extruder, serves

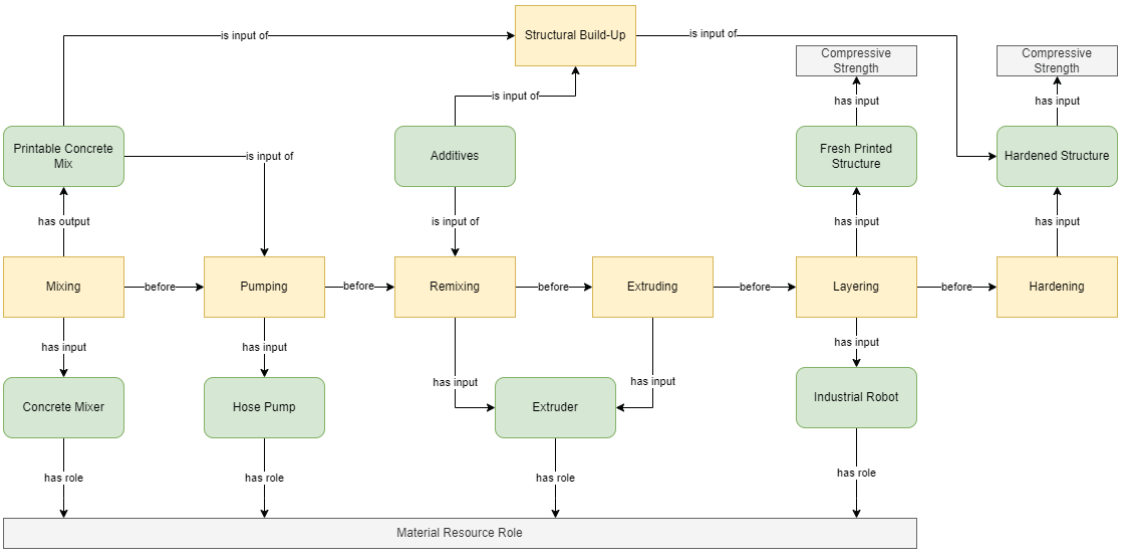

Figure 3.3: Concept of Manufacturing Process

a purpose for the given process; thereby, they are defined as roles within the ontology. The properties are defined within these roles to describe the capacity/restrictions of its functionality; for example, the structural properties of the printed structure, or the extruder's speed capacity.

3.3.2 Data Query

Validating the correctness of the formalized knowledge base can be done through running SPARQL queries against the ontology to verify that it properly captures the intended knowledge. The following query ((Algorithm)) is an example of the used query aimed to extract detailed information about specific concrete mixtures used in testing processes. It focuses on prescribed concrete specifications, and the results from a slug test. The query retrieves the concrete specification details, the density of the fresh concrete, and the values obtained from the slug test.

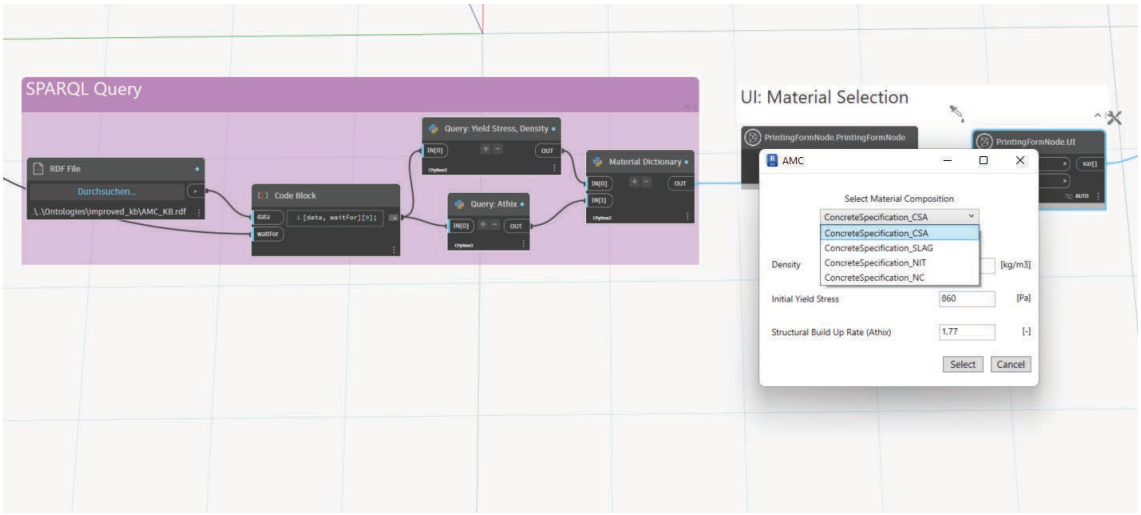

Figure 3.4: Selection of printing mix accessed from the AM ontology

Algorithm 3.1: Retrieval of Material Properties Through SPARQL Query

```
1  PREFIX material: <http://quantecton.com/kb/printing-material#>
2  PREFIX rdf: <http://www.w3.org/1999/02/22-rdf-syntax-ns#>
3  PREFIX owl: <http://www.w3.org/2002/07/owl#>
4  PREFIX rdfs: <http://www.w3.org/2000/01/rdf-schema#>
5  PREFIX xsd: <http://www.w3.org/2001/XMLSchema#>
6  PREFIX iof: <https://spec.industrialontologies.org/ontology/
       core/Core/>
7  PREFIX obo: <http://purl.obolibrary.org/obo/>
8  PREFIX modal: <http://quantecton.com/kb/modalRelation/>
9  PREFIX qudt: <http://qudt.org/schema/qudt/>
10
11 select ?concreteSpec ?concreteDensityValue ?
       stressValueApproximatedBySlugTest ?stressUnit where {
12         ?concreteSpec a material:
               PrescribedConcreteSpecification .
13         ?concreteSpec modal:prescribes ?
               prescribedPortionOfMaterial .
14         ?concreteSpec iof:prescribes ?freshConcreteForSlugTest
               .
15         ?freshConcreteForSlugTest a material:
               PortionOfFreshConcrete .
16         ?freshConcreteForSlugTest iof:isInputOf ?
               slugTestProcess .
17         ?slugTestProcess iof:hasOutput ?stressValueFromSlugTest
               .
18         ?stressValueFromSlugTest iof:hasSimpleExpressionValue ?
               stressValueApproximatedBySlugTest .
19         ?prescribedPortionOfMaterial a material:
               PortionOfFreshConcrete .
20         ?prescribedPortionOfMaterial modal:hasQuality ?
               concreteDensityParam .
21         ?concreteDensityParam a material:ConcreteFreshDensity .
22         ?concreteDensity modal:isMeasuredValueOfAtSomeTime ?
               concreteDensityParam.
23         ?concreteDensity iof:hasSimpleExpressionValue ?
               concreteDensityValue .
24         ?stressValueFromSlugTest qudt:unit ?stressUnit .
25 }
```

Information retrieved through these queries is integrated into the BIM/FIM project. Specifically, the knowledge base provides detailed information on the material properties of concrete mixtures. An example was taken from an experiment presented by MIRANDA et al. (2023), which explored these mixtures from a rheological perspective, outlining properties such as shear-thinning viscosity, reversible-irreversible plasticity behavior, and both static and dynamic yield stress. Understanding these properties is aimed to determine the proper balance of material composition, open time, robot speed, and filament dimensions, to avoid layer deformation from self weight, weight from successive layers, and nozzle induced stress.

The integration with the FIM framework is performed within Dynamo, where the queries are expressed in a Python script using RDFLib to manage graph data and execute SPARQL queries for extracting data based on specific patterns. The queried knowledge supports FIM framework, allowing to specify the selected material. The chosen material with its correlated properties are key factors that determines appropriate process information for fabrication. To facilitate the selection process, a user interface was developed using ZeroTouch nodes, displaying the queried knowledge as a dropdown list which then passes through the values for analysis elaborated in Section 3.4 (Figure 3.4).

3.4 Applied Analytical Models

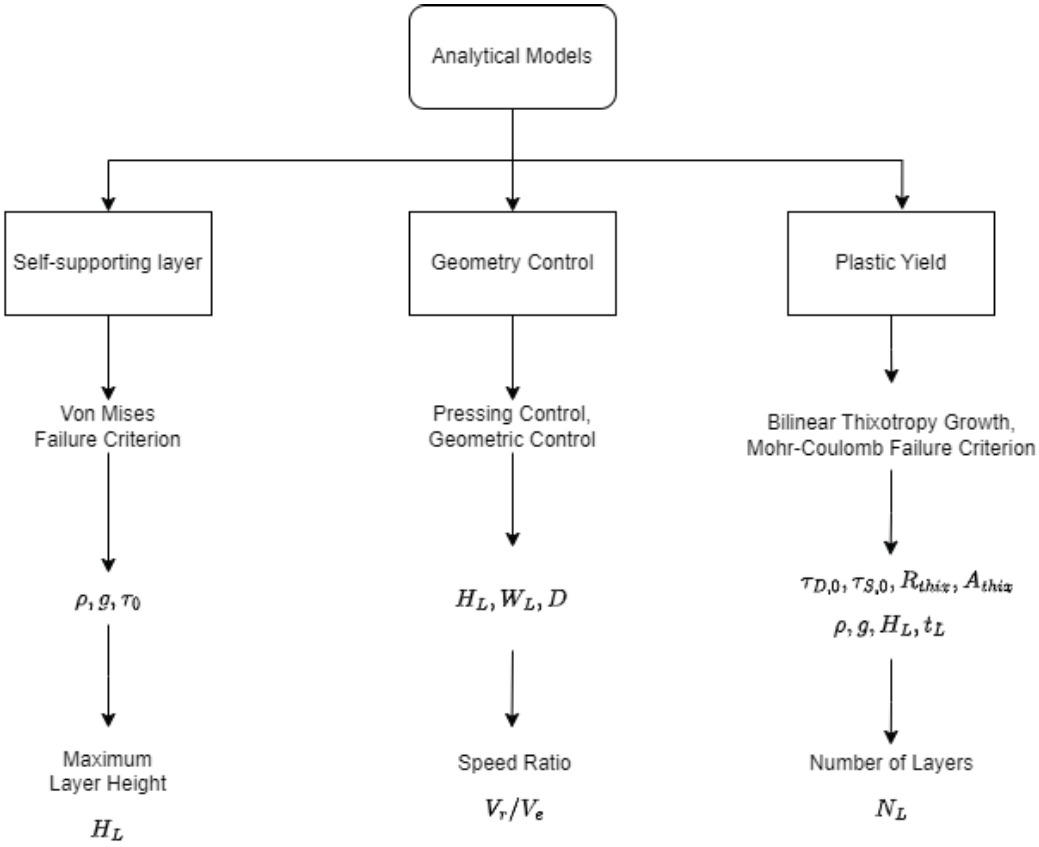

Figure 3.5: Overview of the analytical models implemented in the FIM framework

The analytical models presented in Figure 3.5 are applied in the FIM framework to retrieve appropriate process parameters to enhance the success rate of printing. For simplicity due to time constraints, the focus of this analysis is restricted to vertical building elements on a planar printing surfaces. TBoundary conditions are established, aimed to ensure shape retention of self-weight, geometric control, and buildability against plastic collapse. Derived from the theoretical framework presented by Carneau and Kruger, the boundary conditions are defined as follows:

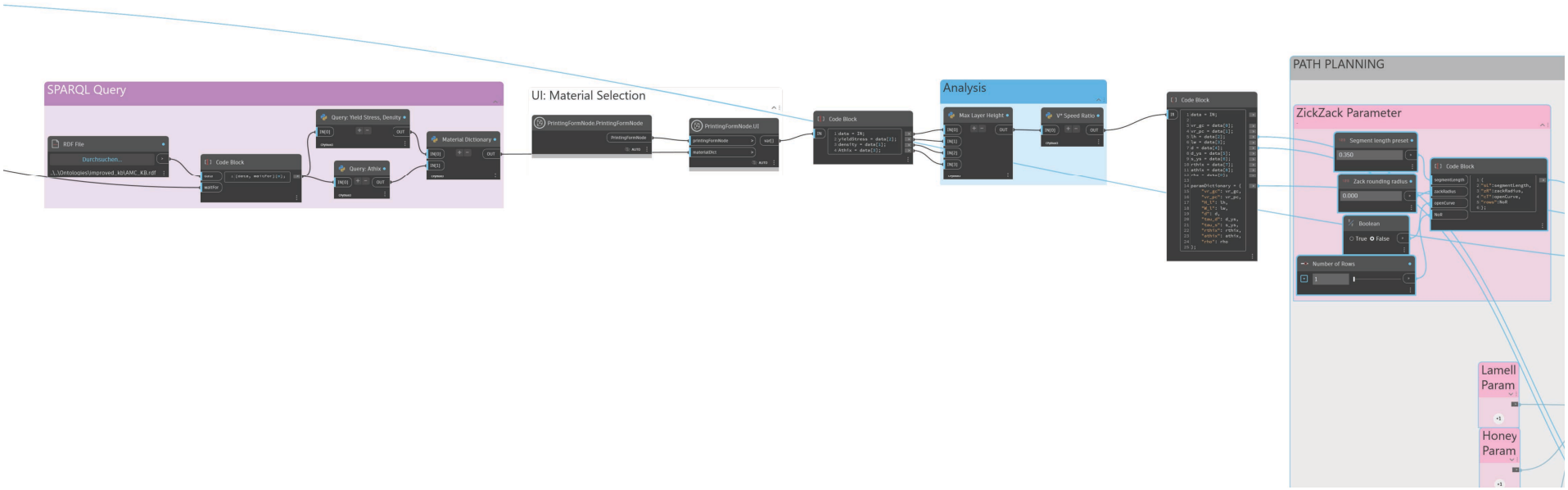

Figure 3.6: Dynamo graph of the embedded analytical model in relation with the SPARQL Query from the AMC knowledge base

3.4.1 1st Boundary Condition: Self-Supporting Layer

Starting from the deposition of the material, the printed layer must be capable to sustain its own weight to prevent deformation and maintain structural integrity. This requirement is quantified using the relative layer weight parameter $\omega^* = \frac{\rho g H}{\tau_0 \sqrt{3}}$, which expresses the normal stress relative to the material's yield strength under Von Mises failure criterion (refer to Section 2.2.2). For the layer to be self-supporting, ω^* must be less than 1. Therein, a maximum layer height H can be obtained:

$$H_{Lmax} = \frac{\tau_0 \sqrt{3}}{\rho g} \tag{3.1}$$

3.4.2 2nd Boundary Condition: Pressing and Geometric Control

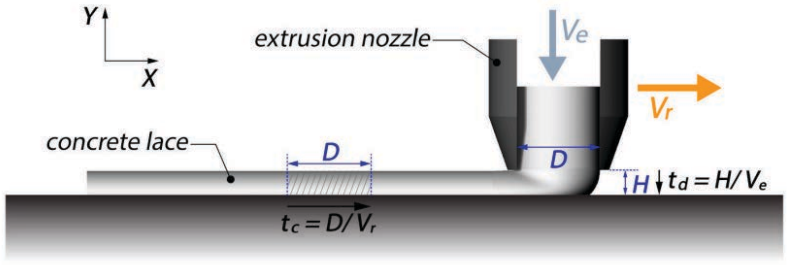

Figure 3.7: Printing Parameters for Pressing Control (CARNEAU et al., 2022)

The following kinematic analysis establishes the conditions for extrusion to achieve geometric conformability through layer pressing. Within the layer pressing regime, an extrusion is considered pressed if the material reaches the substrate before the nozzle moves further. As illustrated in Figure 3.7, two types of time parameters are key within the pressing regime: $T_r = \frac{D}{v_r}$, which determines the duration a point remains under the nozzle; and $T_d = \frac{h_L}{v_e}$, which represents the time required for the material to exit the nozzle and reach the base surface. These parameters set a critical standard to prevent longitudinal tearing of the extrusion.

$$\frac{H_L}{V_e} < \frac{D}{V_r} \tag{3.2}$$

With the dimensionless parameters $H^* = \frac{H_L}{D}$ and $V^* = \frac{V_r}{V_e}$, the boundary condition for pressing control proposed in CARNEAU et al. (2022) model suggests $H^*.V^* < 1$. Given the layer dimensions as input parameters, the speed ratio can be expressed in the following relation:

$$V^*_{PC} < \frac{D}{H_L} \tag{3.3}$$

However, in cases where the desired layer width exceeds the nozzle diameter, it is necessary to extend the pressing duration in order for the nozzle printer to overextrude

to achieve the intended layer width. The law of mass conservation ensures that the mass of material extruded aligns with the chosen dimensions of the printed object. It is represented by the equation $S_L.V_r = S_N.V_e$, where S_L denotes the cross-sectional area of the filament and S_N as the Nozzle's cross-section area. To take account for the filament's non-rectangular cross-section, a corrective coefficient β is applied.

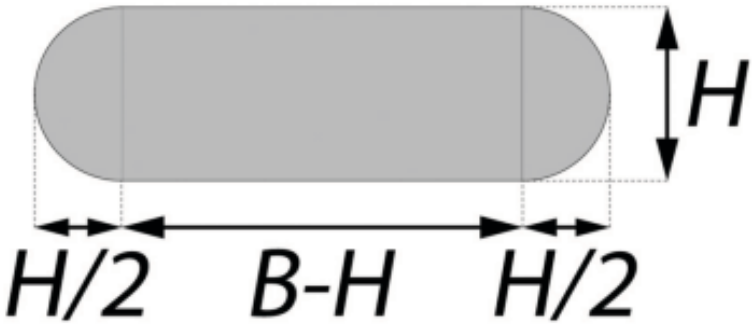

Figure 3.8: Oblong profile of the filament's cross-section (CARNEAU et al., 2022)

The assumption of the extruded filament is depicted in Figure 3.8. In the layer pressing analysis proposed by CARNEAU et al. (2022), the speed ratio under basis of the mass conservation is derived as $V^*_{GC} = \frac{\pi}{4\beta.H^*.B^*}$; with B^* as the dimensionless width parameter equivalent to B/D. Substituting β that is derived in the analysis proposed, the velocity ratio for geometric control can be retrieved:

$$V^*_{GC} = \frac{\pi}{H^*.(4.B^* + (\pi - 4)H^*)} \tag{3.4}$$

This analysis conclude the 2nd boundary condition for kinematic control, which offers two values: the upper bound V^*_{PC} that ensures pressing control to prevent longitudinal tearing, and the lower bound V^*_{GC} that facilitates achieving the intended filament dimension.

3.4.3 3rd Boundary Condition: Plastic Yield Failure

As outlined in Section 2.2.3, the model presented by Kruger addresses one of the structural failure mechanisms, plastic collapse, which occurs when the building rate surpasses the time-dependent material shear strength. Taking into account that the material structural build up is characterized by two phases: reflocculation and structuration, it must be firstly determined whether failure happens during flocculation or structuration. Thereby, a comparison should made between the gradient of the building rate and the material-specific fixed gradient (Figure 3.9).

The building rate defined as $\tau(N_L) = \frac{\rho.g.H_L.N_L}{2.F_{AR}}$, where if the total printing time t is expressed in N_L, then t can be expressed as $t = t_L.N_L$. Transforming N_L into a function of time, we can retrieve $\tau(t) = \frac{\rho.g.H_L}{2.F_{AR}.t_L}.t$, which allows to calculate the gradient of the building rate as $\frac{d\tau}{dt}$.

Algorithm 3.2: Assess maximum number of layers

```
def getCrit_N_Layers(layer, tau_d: float, tau_s: float, R_thix: float, l_p: float,
rho: float, g: float, H_L: float, F_AR: float, A_thix: float, layerTime: float) -> Tuple[float, np.ndarray, float, np.ndarray, float]:

dtau_dt = (rho * g * H_L ) / (2 * F_AR * layerTime) # Building rate
m_mat = (tau_d * R_thix) / (tau_s - tau_d) # Material specific gradient

if dtau_dt >= m_mat:
numerator = tau_d
denominator = (R_thix * layerTime) - ((rho * g * H_L) / (2 * F_AR))
else:
numerator = tau_s + (A_thix * (tau_d - tau_s)) / A_thix
denominator = (A_thix * layerTime) - ((rho * g * H_L) / (2 * F_AR))

N_L = - (numerator / denominator)
return N_L
```

Furthermore, the material-specific gradient is determined between the coordinates (0,0) and the transition point $(t_{rf}, \tau_{S,i})$. Therefore, the comparison between material specific gradient and the building rate gradient can be expressed:

$$\frac{d\tau}{dt} \geq \frac{\tau_{S,i}.R_{thix}}{\tau_{S,i} - \tau_{D,i}} \tag{3.5}$$

Depending on the inclination of the building rate, if Eq.3.5 applies, then failure is likely to occurs during re-flocculation in which the number of layers can be quantified:

$$N_L = -\left[\frac{\tau_{D,i}}{R_{thix}.t_L - \frac{\rho.g.H_L}{2.F_{AR}}}\right] \tag{3.6}$$

Whereas if the failure occurs during structuration:

$$N_L = -\left[\frac{\tau_{S,i} + \frac{A_{thix}(\tau_{D,i} - \tau_{S,i})}{A_{thix}}}{A_{thix}.t_L - \frac{\rho.g.H_L}{2.F_{AR}}}\right] \tag{3.7}$$

This boundary condition determines the maximum number of layers that can be printed before plastic collapse, which is dependant on the material properties and the process parameters (H_L, t_L). The flexibility of this analysis allows for adaptation based on desired outcomes. Additionally, there remains the possibility to adjust the layer time according to the specified number of layers, offering further customization in the construction process.

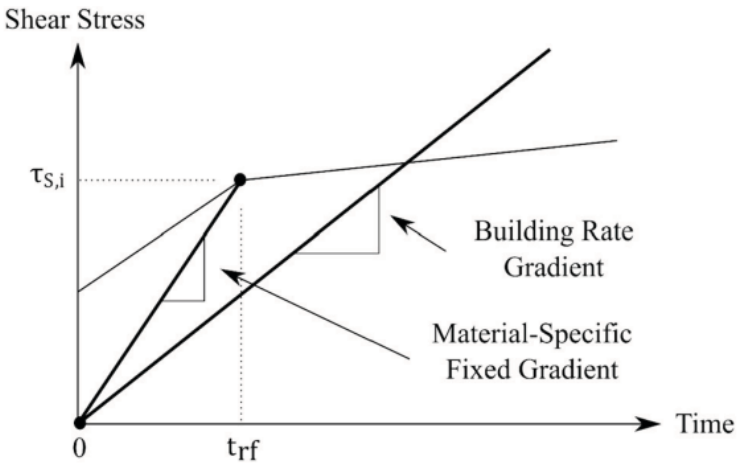

Figure 3.9: Building rate gradient and material-specific gradient (KRUGER, ZERANKA, & ZIJL, 2019)

3.5 Manufacturability Analysis

Focused on an AM method using stationary industrial printing robots, it is essential to determine whether the modeled building objects falls within reach of the robot's workspace boundaries. The KUKA KR 210, an industrial robot model with 6 DOFs and a maximum reach of 4.25 m in height, was chosen for this analysis.

Utilizing the capabilites of the Revit API to retrieve the geometric information within a BIM project, an estimation of the manufacturability can be performed through examining the geometric information of the building elements and the robot's bounding volume. The objective of the estimation is to ensure the robot's workspace geometry and the modelled object fully intersect in 3D or 2D. This is achievable using Dynamo Revit, which accessess the Revit API, allowing for transformations such as translations and rotations on geometric elements within the Dynamo environment. It also provides standard methods such as intersection checks between different geometric elements. Thus, this process is embedded in the FIM framework in Dynamo, set at the initial step of the Dynamo script before it runs the analytical model (Section 3.4), and generates the print path model.

The initial approach was to analyze in 3D whether the solid of the modeled wall fully intersects with the robot's workspace. The volume of the robot's workspace represents roughly a half-sphere solid with a inner void that defines the volume occupied by the robot itself (refer to Figure 3.10). A downside of Dynamo is that it interprets void as solid, resulting in inaccuracies when checking the net intersection volume of the two solids.

A workaround for this challenge is to perform the estimation in a 2D perspective. By taking the cross-sectional area of the workspace at the height of the building element with an additional gap distance for safety, a minimum/lower bound range of the bounding cross-section area can be established (Figure 3.11). The cross-section area of the robot's workspace is represented as a donut-shaped area, where the inner circle is defined as the space occupied by the printer itself.

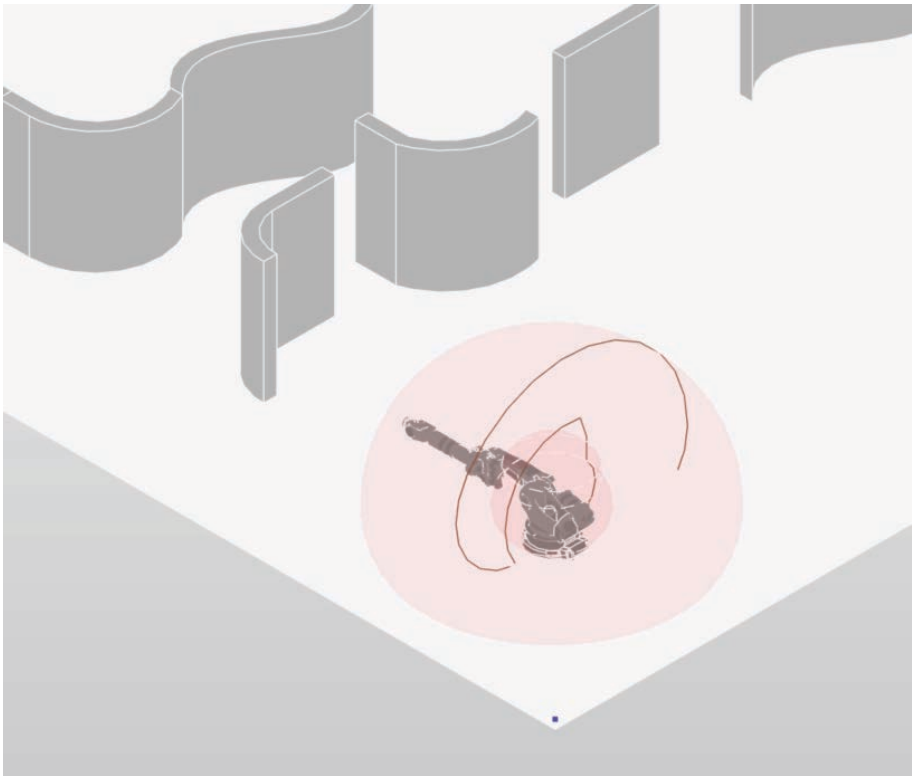

Figure 3.10: Geometry model of robot workspace and sample walls for manufacturability analysis

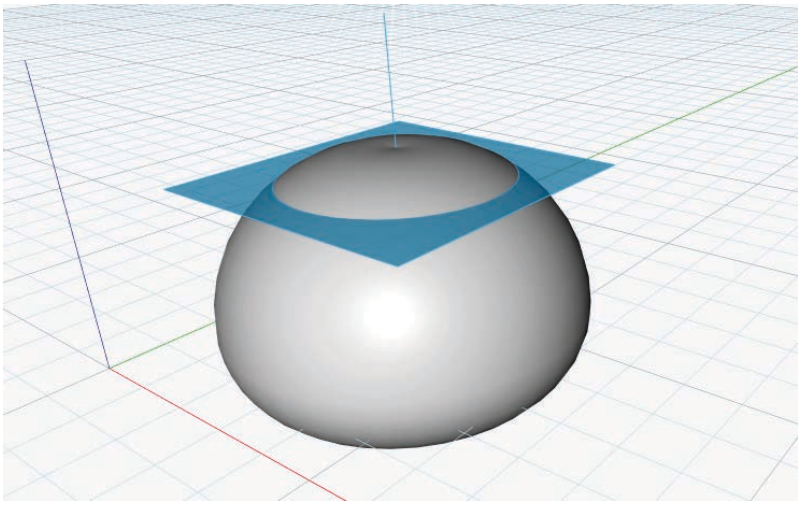

Figure 3.11: Retrieval of 2D cross-section plane of the robot workspace based on the height level of the building element

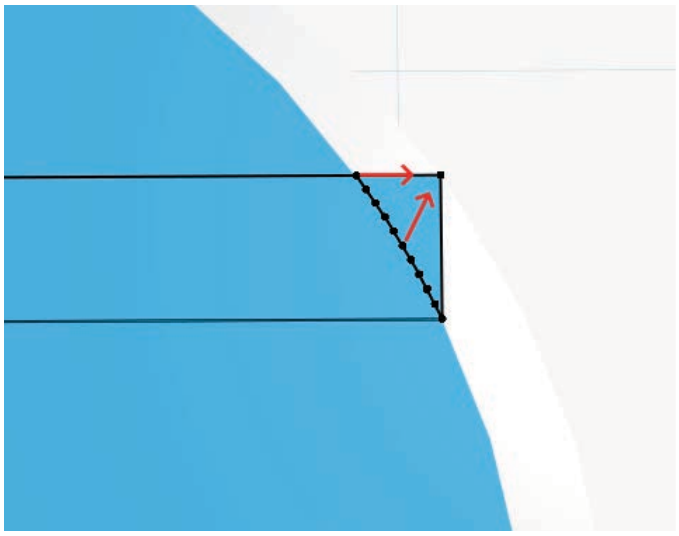

Figure 3.12: Iteration of translation points to achieve full intersection

Algorithm 3.3: Shift robot workspace in incremental steps for a complete intersection (Fig. 3.12)

```
- Calculate intersection area between RobotWS and Wall.
- IF the difference of intersection < tolerance THEN
        - The current position of RobotWS is optimal.
- ELSE
        - Get cutout edges from the difference geometry and get
            sample points [a] along its curve.
        - Get overlapping curve of the cutout edge and the
            outer perimeter of RobotWS, and get sample points [
            b] along its curve.
        - WHILE the intersection area is not optimal DO
                - Translate RobotWS using the vector based on
                    sample points [a] to [b].
                - Update the maximum intersection area if found
                    within loop.
                - IF the maximum intersection area equals the
                    wall area THEN
                        - BREAK the loop.
                - ELSE
                        - Recalculate the intersection area
                            between RobotWS and Wall.
```

The estimation goes through three iterative steps of checks (refer to Figure 3.13): (a) positioning at the mid-point, (b) aligning both inner curves of robot's workspace and wall, (c) adjusting to fit. Initially, the mid-points of both wall cross-section surface and the robot workspace are positioned together in the Dynamo environment. Then, to maximize the intersection area, the inner curves of both the printer's workspace and the wall are aligned. Depending on the wall's dimensions, any overlapping areas from the intersection are further analyzed. Thereby, the process proceeds through iteratively adjusting the position of the robot's workspace to maximize the intersection are with the modeled wall. This involves determining the outermost points of the cutout edges created by the difference between the wall and the robot's workspace, utilizing these points as reference for translation. Retrieving the optimized position is repeated for a specified number of iterations. If any overlapping surface after the iteration process persists, the user is notified that the wall dimensions exceeds the bounding area of the robot workspace.

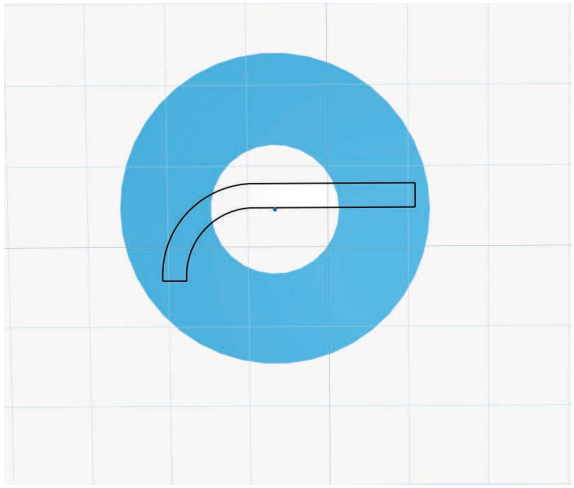

(a)

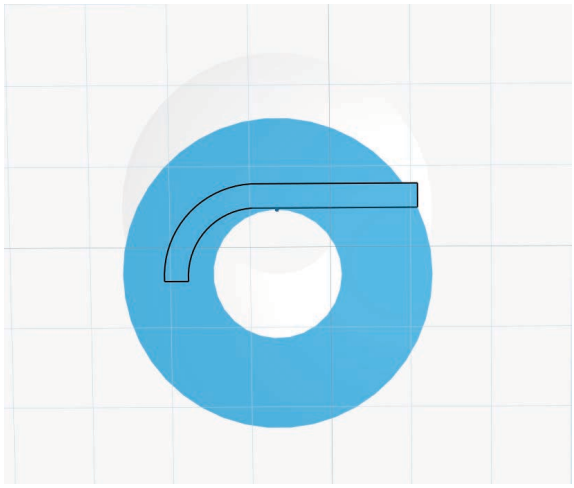

(b)

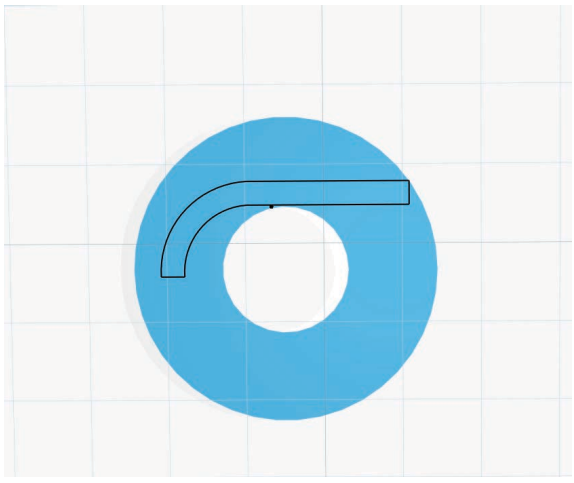

(c)

Figure 3.13: Manufacturability Analyis: (a) Position center points of robot workspace and wall, (b) Align inner perimeter of robot workspace to wall center point, (c) Adjust wall through iterations of translations

Chapter 4

Experimental Study

4.1 Material Test

Figure 4.1: Penetration Test on Clay Mix

The material used for this experiment is the boesner Terra 502 block of clay. It consists of purely kaolinitic clay with a density of 2,6 g/cm^3. For the printing process, the clay mixture comprises 1000 gr clay with 400 gr water. To determine the necessary material properties for the analytical model, a penetration test is conducted. This test is essential for evaluating the continuous yield strength growth of fresh concrete.

A novel penetration test method introduced by C. MAXIMILIAN HECHTL (2024) proposes combining Fast Penetration (FP) and Slow Penetration (SP). In this method, the conical tip is initially driven into the material at a high velocity and then transitions at a much slower velocity after a period of seconds. The FP phsae helps to retrieve the force required to overcome sliding friction, in which the dynamic yield stress can be determined. Whereas the SP represents the force to overcome static friction, directly attributed to the static yield stress.

During the test, normal forces were recorded and the results are outputted in a spreadsheet format. The yield stress is examined based on the tabular data of forces (F) recorded at each timestamp with a duration of 45 minutes. The conical tip utilized in the test had an angle of 30°, a diameter (D) of 15 mm and a height (H) of 27.99 mm.

$$\tau_0 = \frac{F}{\pi.R.\sqrt{R^2 + H^2}} \tag{4.1}$$

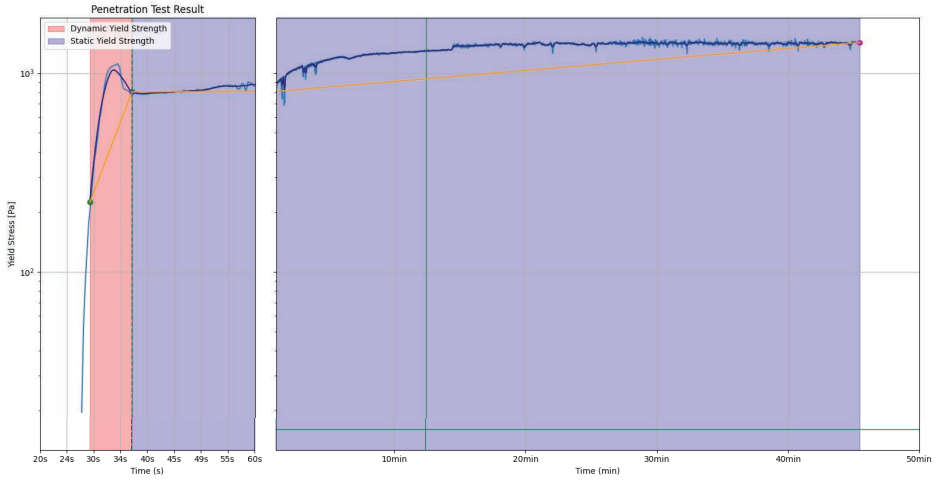

Figure 4.2: Evaluated Yield Strength Growth of Clay Mix from Penetration Test

The initial spike observed in the curve is attributed to the drastic change in the velocity of the conical tip. It takes a brief moment for the force to stabilize, overcoming the sliding friction. The results indicate a gradual increase in yield strength, with rapid initial growth representing the dynamic yield strength. This growth is influenced by the fast flocculation rate (R-thix). After a short period of time, a steady state is achieved, as indicated by the change in the gradient of yield strength growth, which then represents the static yield stress.

Parameter	Value
$\tau_{D,0}$	227 Pa
R_{thix}	16.25 Pa/s
$\tau_{S,0}$	910 Pa
A_{thix}	0.2 Pa/s

Table 4.1: Penetration Test Result

As elaborated in Section 3.4.3, the evaluation of the material resistance utilizes the bilinear thixotropy growth model. Thereby, three critical points to define the bilinear model were identified based on a visual analysis of the plotted graph. After the curve stabilizes, the

starting point (SP) was selected as the initial dynamic yield strength $\tau_{D,0}$. The transition point (TP) was selected at the shift in inclination. The TP was defined as the transition from the dynamic yield strength at the given timestamp $\tau_{D,t}$ to the initial static yield stress $\tau_{S,0}$. The end point (EP) is defined as the static yield stress at its final value τ_S. In addition, the thixotropy rates (R_{thix}, A_{thix}) that denotes as the growth rate of the yield strength per second, represents the gradient of the plotted bilinear model for respectively dynamic and static yield strength.

As elaborated in Section 3.4.3, the evaluation of the material resistance utilizes the bilinear thixotropy growth. Thereby, three critical points to define the bilinear model were required and were manually taken based on the visual interpretation of the plotted graph. After the curve line stabilizes, the starting point (SP) was selected as the initial dynamic yield strength $\tau_{D,0}$. The transition point (TP) was selected where the shift of the inclination occurs. It is also visible that after the TP, there is more noise in the record when overcoming the static friction. To reduce noise in the given data, `smoothdata` from MATLAB is implemented, in which it computes the moving average in a specified window size (i.e., time span). The TP was defined as the transition from the dynamic yield strength at the given timestamp $\tau_{D,t}$ and the initial static yield stress $\tau_{S,0}$. Lastly, the end point (EP) represents the static yield stress at the last value τ_S. In addition, the thixotropy rates (R_{thix}, A_{thix}) that are defined as the growth rate of the yield strength per second, represents the gradient of the plotted bilinear model for respectively dynamic and static yield strength.

4.2 3D Printer

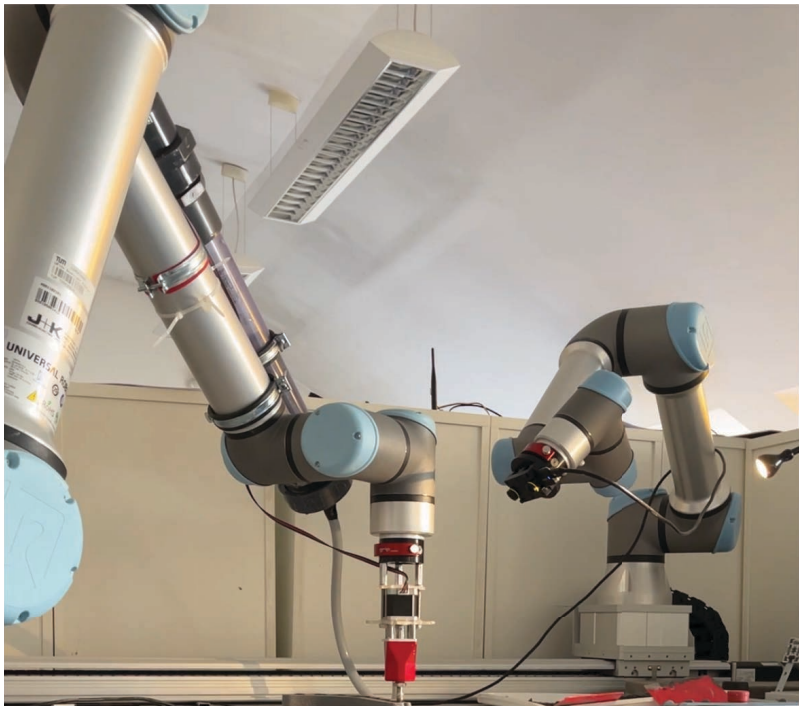

Figure 4.3: UR10e Industrial Robot

The Universal Robot UR10e was implemented as the industrial arm robot for the experimental work. It has a reach of 1300 mm and a payload capacity of 12,5 kg and movement ability with 6 degrees of freedom. It allows to be controlled with its native software, Polyscope. Furthermore, the controller data can also be sent through TCP/IP to Polyscope, thereby allowing to send information of the positioning and movement of the robot arm for printing.

In addition, a ram extruder is coupled onto the robot arm. It is a cartridge that transports the printing material, in which it is extruded with a piston that its movement is coupled with the screw on a threaded rod. The rotation of the rod is controlled through a stepper motor, thus, moving the piston and shoves material through the pipe to the nozzle head, StoneFlower3D, a ceramic nozzle head that extrudes paste-like material. The movement is defined from the controller that sends the extrusion rate to Arduino that sets the rotation for the stepper motor.

4.3 Setup

In this experiment, the printing setup was configured to ensure optimal printing conditions. The layer printing time was set to 60 seconds, allowing for adequate time for the layers to stiffen without compromising the print speed. The velocity profile was calibrated to the curvature of the print path layout, restricted by the maximum acceleration of 0.15 mm/s and the given layer time (see Figure 4.4). Furthermore, with the analysis of plastic failure without considering elastic buckling, the geometry was ensured that it would not influence in the collapse. Thereby, a small aspect ratio was chosen with the layer height of 2 mm and layer width of 6 mm.

4.4 Result

The modelled wall in Revit was brought into realization with a scale factor of 0.1 for the printed size. Prior to printing, it was firstly analyzed within Dynamo to retrieve appropriate parameters (L_H, V^*, and N_{Layers}). With the layer height conforming with the maximum boundary due to the small scaling factor, and the speed ratio conforming the mass conservation principle and not exceeding the upper boundaries of the pressing control, it gave a clean stable outcome of the print result throughout the process. The predicted number of layers that it can withstand before plastic collapse amount to 62 layers. Approximately at 62 layers, the printed structure was recorded as depicted in Figure 4.5. Not long after exceeding the given boundary condition, it collapsed at the 65th layer due to plastic collapse at the bottom critical layer.

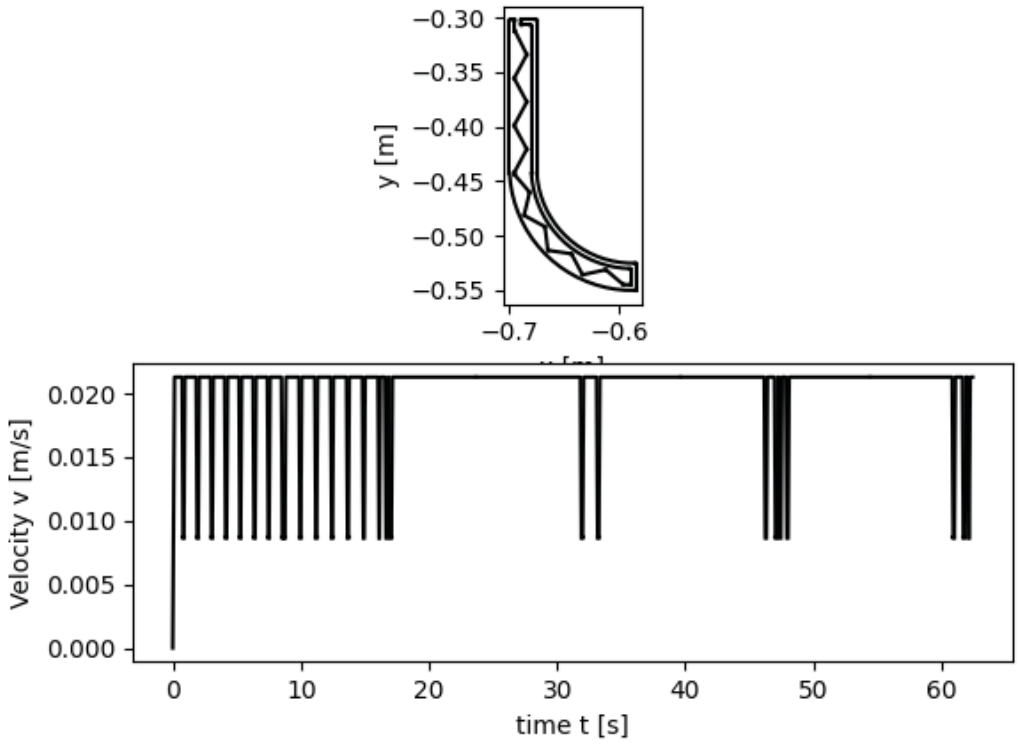

Figure 4.4: Velocity Profile of the Print Path

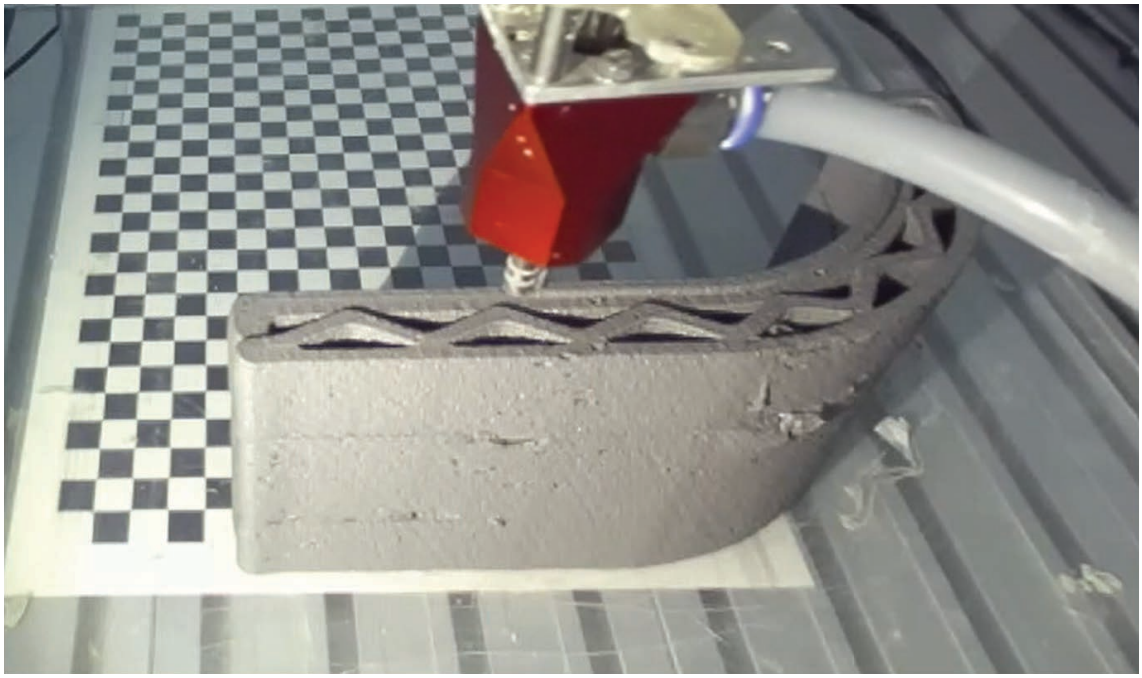

Figure 4.5: Printed Curved Wall at 62 Layers

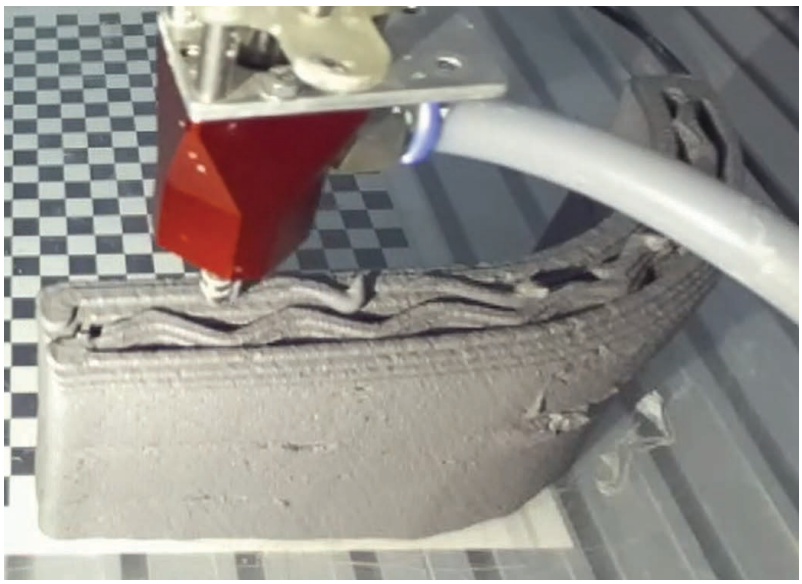

(a)

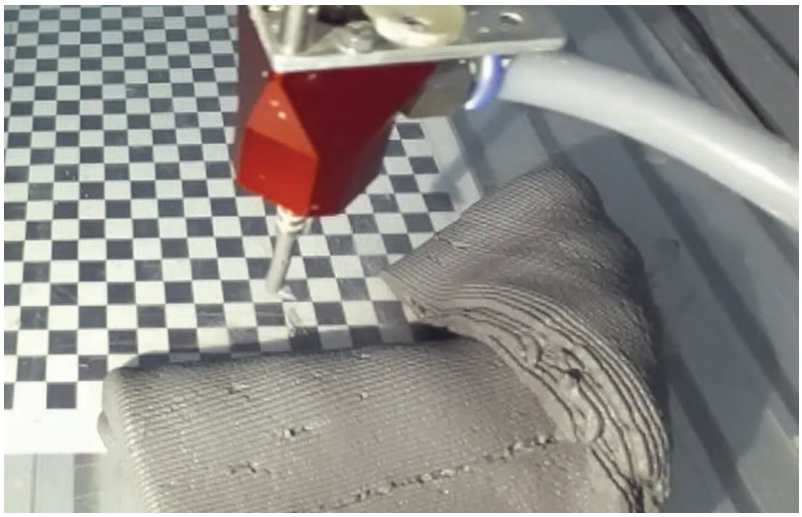

(b)

Figure 4.6: Print result due to plastic failure. (a) Structure leaning away, unaligned from the print path. (b) Immediate collapse split seconds after

Chapter 5

Discussion

The study has provided valuable insights for specific use cases in the early design phase of AMC, integrating the potential use of the AMC knowledge base with the FIM framework. With the scope and challenges defined in Chapter 1, one use case involves analyzing the bounding reach of the printer's workspace to verify the feasibility of design sizes for printing. Another use case focuses on delivering appropriate process information for fabrication to ensure shape conformity and buildability, taking into account the properties of 3DCP materials and kinematic aspects. The following sections discuss the progression of this study:

Knowledge Base

Throughout this study, adjustments to the knowledge base were necessary as new information was occasionally added during the development. The DUL upper ontology is referenced as a solid foundation which the AMC ontology is aligned to; thus, ensuring consistency and allowing for the extension of heterogeneous information. The knowledge base supported the analytical model embedded in the FIM framework, facilitating retrieval of information about concrete mixtures and their material properties.

The AMC knowledge base developed with semantic web technology has its potential to provide shared knowledge for architects and engineers during the design planning stages. It offers an open source for organizing, updating, and retrieving knowledge using complex queries. By storing information, such as material or process data proven successful in printing, the knowledge base allows for reuse of this information, thereby minimizing iterations in design decisions.

Printing Boundary Conditions

In the fabrication process, deposited materials must meet certain criteria as outlined in Section 2.2: pumpability, extrudability, geometric conformity, and buildability. This study established boundary conditions for a controlled printing process, based on geometric conformity and buildability, and referenced from the analytical models by Carneau and Kruger.

The boundary conditions for the process information were defined with basis of the material properties. The first condition ensures the printed filament to support its self-weight.influenced mainly by layer height, which determines the volumetric mass and maximum allowable height.

The second condition sets the upper bounding value of speed ratio (robot speed to extrusion speed) that ensures the layer pressing strategy, avoiding longitudinal tearing (from an over-exceeding high robot speed in relative to extrusion speed). Furthermore, in cases where the robot speed needs to be tuned down in order for the deposited filament to extrude accordingly to the desired layer width, the second boundary condition also proposes a lower bounding value to maintain the geometric control condition, under the principle of the mass conservation, influenced by layer dimensions and nozzle diameter.

The third boundary condition takes account of the buildability of the printed structure. While buildability has two major failure mechanisms—elastic buckling and plastic failure—this study focuses only on plastic failure due to time constraints. It considers the material yield strength's evolution as a bilinear model to approximate material yield strength evolution, intentionally underestimating strength capacity to enhance construction safety. Furthermore, the acting load is assumed to have constant value throughout each layer which results in a linear building rate. With this assumption, only planar print paths was taken into consideration. The boundary condition was evaluated by comparing the evolution of material yield strength against the building rate, predicting that the bottom critical layers will fail once the building rate exceeds the yield strength's growth. Thixotropic properties of the material, influenced by its composition, play a significant role in this outcome. Furthermore, adjusting the process information can fine-tune the feasibility of the total number of printed layers. Reducing layer height permits a gradual increase in the building rate, allowing lower layers time to develop dependent yield strength while progressively resisting smaller incremental loads. Adjusting layer time also affects the time-dependent material's yield strength growth. However, extending layer time excessively may weaken the Interlayer Bond Strength (IBS), as surface moisture of the deposited layer may evaporate depending on external environmental factors, thereby reducing the IBS value (MOELICH et al., 2021).

Bounding Reach of the Robot's Workspace: Manufacturability Analysis

The early stages of design benefit significantly from streamlined and efficient validation processes. The manufacturability of building objects with stationary industrial robots was assessed using a conservative geometric and algorithmic approach by checking the intersections of the BIM models.This method quickly iterates and modifies designs without heavy computational demand. Given the uncertainties inherent in early design stages- such as incomplete data of operational constraints, this method takes a buffer by overestimating the spatial needs, which minimizes risks within the validation. However, this may obscure more optimized design pathways, overlooking the full capabilities for printing. In future stages of the project, where more detailed data are available, transitioning to more precise simulation-driven methodologies would be beneficial to optimize the design.

Chapter 6

Conclusion and Outlook

6.1 Conclusion

In this study, a streamlined knowledge-to-fabrication approach was implemented, utilizing the AMC formal knowledge to support the planning process within the FIM. Information on material compositions for 3DCP and its mechanical properties—including density, initial yield strength, and thixotropy rate—was extracted through SPARQL queries from the knowledge base. Analytical models to maintain geometric conformity and buildability were developed within the FIM framework, utilizing the queried information. These models factor in the rheological behaviors of concrete printing materials using a bilinear thixotropy model, consider plastic yield under the Mohr-Coulomb failure criterion, and incorporate printing parameters. The combination of these factors influences the output of printing quality, which sets boundary conditions specifying maximum layer height, speed ratio, and maximum number of layers.

6.2 Future Studies

While the methods employ conservative estimations for early design stages to minimize computational burden, refinements and wider exploration should be looked further. In the context of manufacturability, the method proposed by Son and Kwon (2019) involves using a convex programming approach to optimize the base position of a 6-Degrees of Freedom (DOF) robot with a spherical wrist. This method provides a more accurate assessment of reachability and determination of base position, without the need to solve inverse kinematics; thus, minimizes complexity in computation.

Implemented experiments have utilized clay mix, which does not entirely represent the rheological behaviors of concrete mixtures. Unlike clay, which cures through a physical drying process, concrete cures chemically, forming CSH and Calcium Hydroxide (CH) that plays a critical role for the development of the strength and durability of the material. In addition, the time-dependent elastic modulus of concrete should be considered into the analysis, as it influences the material's strain under stress. Each layer experiences strain from its own weight and the cumulative weight of subsequent layers, leading to progressive deformation.

To fully harness the full potential of 3DCP in regard to geometric freedom, the feasibility of non-vertical 3D printed objects should as next step be assessed, taking into account eccentricity and plausibly requiring a numerical approach due to geometric complexity. In

addition, a study conducted by SUIKER et al. (2020) explored elastic buckling on different wall conditions, including free-standing wall, simply supported wall, and fully-clamped walls, which each condition affects the buckling behavior. The study proposes a parametric model to predict critical buckling length, considering factors such as the wall's geometry, the curing rate, and imperfections on the structure.

Furthermore, it is necessary to understand how environmental factors and layer time influence the IBS over time. Investigations by (MOELICH et al., 2021) have revealed that surface moisture significantly affects the bond strength between layers, which is a critical factor that can be modified by incorporating additives into the concrete layers. Additionally, the application of fresh cement paste mixed with various admixture agents can notably enhance both IBS and compressive strength, potentially increasing the latter by up to 60% (MARCHMENT et al., 2019). These studies emphasize the importance of controlling environmental conditions and adjusting layer times to optimize the structural integrity and durability of 3D printed concrete structures

From the given challenges, it can be observed that the planning for AMC is inherently complex. As the field continues to undergo intensive research and standardized methods are yet to be established, there is a necessity to enhance the accuracy and integrity of the knowledge base. It should be continually updated through a feedback based on the quality of printed results; for example, considering material compositions, process information, and environmental factors. This will create a closed feedback loop in the design process, constantly optimizing the accuracy and relevance of the knowledge base.

Bibliography

AUTODESK. (2024). Autodesk revit features. https://www.autodesk.com/products/revit/features

BORRMANN, A., KÖNIG, M., KOCH, C., & BEETZ, J. (2018). *Building information modeling : Technology foundations and industry practice*.

BOS, F. P., MENNA, C., PRADENA, M., KREIGER, E., da SILVA, W. R., REHMAN, A. U., WEGER, D., WOLFS, R. J., ZHANG, Y., FERRARA, L., & MECHTCHERINE, V. (2022). The realities of additively manufactured concrete structures in practice. *Cement and Concrete Research*, *156*. https://doi.org/10.1016/j.cemconres.2022.106746

BOS, F., WOLFS, R., AHMED, Z., & SALET, T. (2016). Additive manufacturing of concrete in construction: Potentials and challenges of 3d concrete printing. *Virtual and Physical Prototyping*, *11*, 209–225. https://doi.org/10.1080/17452759.2016.1209867

C. MAXIMILIAN HECHTL, C. G., Thomas Kränkel. (2024). Investigations into the dynamics of penetration tests in digital fabrication [In press].

CAI, L. (2018). On-site autonomous fabrication at architectural scales. https://dspace.mit.edu/handle/1721.1/119078

CARNEAU, P., MESNIL, R., BAVEREL, O., & ROUSSEL, N. (2022). Layer pressing in concrete extrusion-based 3d-printing: Experiments and analysis. *Cement and Concrete Research*, *155*, 106741. https://doi.org/https://doi.org/10.1016/j.cemconres.2022.106741

DAVIS, R., SHROBE, H., & SZLOVITS, P. (1993). What is a knowledge representation. https://courses.csail.mit.edu/6.803/pdf/davis.pdf

DUCOULOMBIER, N., CARNEAU, P., MESNIL, R., DEMONT, L., CARON, J. F., & ROUSSEL, N. (2020). "the slug test": Inline assessment of yield stress for extrusion-based additive manufacturing. *RILEM Bookseries*, *28*, 216–224. https://doi.org/10.1007/978-3-030-49916-7_22/TABLES/2

EASTMAN, C. (2008). *Bim handbook: A guide to building information modeling for owners, managers, designers, engineers and contractors*. Wiley. https://books.google.de/books?id=IioygN0nYzMC

GURSEL DINO, I., SARIYILDIZ, S., STOUFFS, R., & AKIN, O. (2009). Contextual ontology support as external knowledge representation for building information modeling. *Cultures and Visions: CAAD Futures*, 488–500.

HAAR, B. T., KRUGER, J., & van ZIJL, G. (2023). Off-site construction with 3d concrete printing. *Automation in Construction*, *152*, 104906. https://doi.org/10.1016/J.AUTCON.2023.104906

ISO/ASTM 52900: 2021. *Additive manufacturing for construction — qualification principles — structural and infrastructure elements*. 2021. https://www.iso.org/obp/ui/#iso:std:iso-astm:52900:ed-2:v1:en

KEATING, S. J., LELAND, J. C., CAI, L., & OXMAN, N. (2017). Toward site-specific and self-sufficient robotic fabrication on architectural scales. *Science Robotics*, *2*, 8986. https://doi.org/10.1126/SCIROBOTICS.AAM8986

KLOFT, H., GEHLEN, C., DÖRFLER, K., HACK, N., HENKE, |. K., LOWKE, D., MAINKA, |. J., & RAATZ, A. (2021). Trr 277: Additive manufacturing in construction. https://doi.org/10.1002/bate.202000113

KRUGER, J., ZERANKA, S., & van ZIJL, G. (2019). 3d concrete printing: A lower bound analytical model for buildability performance quantification. *Automation in Construction*, *106*, 102904. https://doi.org/10.1016/J.AUTCON.2019.102904

KRUGER, J., ZERANKA, S., & ZIJL, G. V. (2019). An ab initio approach for thixotropy characterisation of (nanoparticle-infused) 3d printable concrete. https://doi.org/10.1016/j.conbuildmat.2019.07.078

KUKA. (2021). Kr 210 r3100 ultra - technical specification. www.kuka.com

LI, C., & PETZOLD, F. (2022). Formal knowledge as a basis for bim-based design decision support in additive manufacturing.

LI, C., ZAHEDI, A., & PETZOLD, F. (2022). Pragmatic design decision support for additive construction using formal knowledge and its prospects for synergy with a feedback mechanism. *Buildings*, *12*. https://doi.org/10.3390/buildings12122072

LOWKE, D., DINI, E., PERROT, A., WEGER, D., GEHLEN, C., & DILLENBURGER, B. (2018). Particle-bed 3d printing in concrete construction – possibilities and challenges [SI : Digital concrete 2018]. *Cement and Concrete Research*, *112*, 50–65. https://doi.org/https://doi.org/10.1016/j.cemconres.2018.05.018

MARCHMENT, T., SANJAYAN, J., & XIA, M. (2019). Method of enhancing interlayer bond strength in construction scale 3d printing with mortar by effective bond area amplification. *Materials Design*, *169*, 107684. https://doi.org/10.1016/J.MATDES.2019.107684

MIRANDA, L. R., JOVANOVIĆ, B., LESAGE, K., & SCHUTTER, G. D. (2023). Geometric conformability of 3d concrete printing mixtures from a rheological perspective. *Materials 2023, Vol. 16, Page 6864*, *16*, 6864. https://doi.org/10.3390/MA16216864

MOELICH, G. M., KRUGER, J., & COMBRINCK, R. (2021). Modelling the interlayer bond strength of 3d printed concrete with surface moisture. *Cement and Concrete Research*, *150*, 106559. https://doi.org/10.1016/J.CEMCONRES.2021.106559

OZTOPRAK, O., SLEPICKA, M., ANINGER, A. L., KOLLMANNSBERGER, S., RANK, E., & BORRMANN, A. (n.d.). Linking fabrication information modeling and finite cell method for simulating the behavior of additively manufactured building components.

PAOLINI, A., KOLLMANNSBERGER, S., & RANK, E. (2019). Additive manufacturing in construction: A review on processes, applications, and digital planning methods. https://doi.org/10.1016/j.addma.2019.100894

PAUWELS, P., ZHANG, S., & LEE, Y. C. (2017, January). Semantic web technologies in aec industry: A literature overview. https://doi.org/10.1016/j.autcon.2016.10.003

PERROT, A., RANGEARD, D., & PIERRE, A. (2016). Structural built-up of cement-based materials used for 3d-printing extrusion techniques. *Materials and Structures/Ma-*

teriaux et Constructions, *49*, 1213–1220. https://doi.org/10.1617/S11527-015-0571-0

Rehman, A. U., & Kim, J.-H. (2021). 3d concrete printing: A systematic review of rheology, mix designs, mechanical, microstructural, and durability characteristics. *Materials*, *14*(14). https://doi.org/10.3390/ma14143800

Reiter, L., Wangler, T., Roussel, N., & Flatt, R. J. (2022). Slow penetration for characterizing concrete for digital fabrication. *Cement and Concrete Research*, *157*, 106802. https://doi.org/10.1016/J.CEMCONRES.2022.106802

Roussel, N., Ovarlez, G., Garrault, S., & Brumaud, C. (2012). The origins of thixotropy of fresh cement pastes. *Cement and Concrete Research*, *42*, 148–157. https://doi.org/10.1016/J.CEMCONRES.2011.09.004

Roussel, N. (2006). A thixotropy model for fresh fluid concretes: Theory, validation and applications. *Cement and Concrete Research*, *36*, 1797–1806. https://doi.org/10.1016/J.CEMCONRES.2006.05.025

Shakor, P., Chu, S. H., Puzatova, A., & Dini, E. (2022). Review of binder jetting 3d printing in the construction industry. *Progress in Additive Manufacturing*, *7*, 643–669. https://doi.org/10.1007/S40964-021-00252-9/FIGURES/8

Slepicka, M., Vilgertshofer, S., & Borrmann, A. (2021). Fabrication information modeling: Closing the gap between building information modeling and digital fabrication. *Proceedings of the International Symposium on Automation and Robotics in Construction*, *2021-November*, 9–16. https://doi.org/10.22260/ISARC2021/0004

Slepicka, M., Vilgertshofer, S., & Borrmann, A. (2022). Fabrication information modeling: Interfacing building information modeling with digital fabrication. *Construction Robotics*, *6*, 87–99. https://doi.org/10.1007/s41693-022-00075-2

Son, S. W., & Kwon, D. S. (2019). A convex programming approach to the base placement of a 6-dof articulated robot with a spherical wrist. *International Journal of Advanced Manufacturing Technology*, *102*, 3135–3150. https://doi.org/10.1007/S00170-019-03391-0/TABLES/4

Suiker, A. S., Wolfs, R. J., Lucas, S. M., & Salet, T. A. (2020). Elastic buckling and plastic collapse during 3d concrete printing. *Cement and Concrete Research*, *135*, 106016. https://doi.org/10.1016/J.CEMCONRES.2020.106016

Wangler, T., Flatt, R. J., Roussel, N., Perrot, A., Sonebi, M., Wolfs, R., Bos, F., Lowke, D., Freund, N., Stephan, D., Pott, U., Reiter, L., Grünewald, S., da Silva, W. R. L., & Schutter, G. D. (2022). Printable cement-based materials: Fresh properties measurements and control. *RILEM State-of-the-Art Reports*, *36*, 99–136. https://doi.org/10.1007/978-3-030-90535-4_4/FIGURES/18

Zhu, B., Pan, J., Nematollahi, B., Zhou, Z., Zhang, Y., & Sanjayan, J. (2019). Development of 3d printable engineered cementitious composites with ultra-high tensile ductility for digital construction. *Materials & Design*, *181*, 108088. https://doi.org/10.1016/J.MATDES.2019.108088

Appendix A

Code

https://gitlab.lrz.de/00000000014ADA7F/fim.git

https://gitlab.lrz.de/00000000014ADA7F/rtde-ur-control.git

Declaration

I hereby affirm that I have independently written the thesis submitted by me and have not used any sources or aids other than those indicated.

Munich, 15.08.2024

Location, Date, Signature